UNIVERSIDAD NACIONAL AUTÓNOMA DE MÉXICO

PROGRAMA DE POSGRADO EN ASTROFÍSICA

Instituto de Radioastronomía y Astrofísica

GENERACIÓN NO ADIABÁTICA DE TURBULENCIA DURANTE EL COLAPSO GRAVITACIONAL

PARA OPTAR POR EL GRADO DE
MAESTRO EN CIENCIAS (ASTROFÍSICA)

PRESENTA
RUBÉN PATRICIO GUERRERO GAMBOA

TUTOR
Dr. ENRIQUE CRISTIÁN VÁZQUEZ SEMADENI (IRyA)

MORELIA, MICHOACÁN AGOSTO 2020

Universidad Nacional Autónoma de México
UNAM
Biblioteca Central
Dirección General de Bibliotecas de la UNAM

UNAM – Dirección General de Bibliotecas
Tesis Digitales
Restricciones de uso

DERECHOS RESERVADOS ©
PROHIBIDA SU REPRODUCCIÓN TOTAL O PARCIAL

Todo el material contenido en esta tesis esta protegido por la Ley Federal del Derecho de Autor (LFDA) de los Estados Unidos Mexicanos (México).

El uso de imágenes, fragmentos de videos, y demás material que sea objeto de protección de los derechos de autor, será exclusivamente para fines educativos e informativos y deberá citar la fuente donde la obtuvo mencionando el autor o autores. Cualquier uso distinto como el lucro, reproducción, edición o modificación, será perseguido y sancionado por el respectivo titular de los Derechos de Autor.

A mis padres Noemí y Rubén ...

Abstract

In my thesis we investigate, both analytically and numerically, the generation of turbulence during the prestellar stages of the gravitational collapse of a turbulent spherical core, in order to determine the fraction of the infall motions that goes into turbulent motions. To do this, we define the ratio $g \equiv \sigma_{\rm 1D}/v_{\rm g}$, where $\sigma_{\rm 1D}$ is the one-dimensional turbulent velocity dispersion, and $v_{\rm g}$ is the gravitational velocity. We then analytically estimate the ratio g under the assumptions of a) equipartition or virial equilibrium between the gravitational ($E_{\rm g}$) and turbulent kinetic ($E_{\rm turb}$) energies and b) stationarity of the transfer from gravitational to turbulent energy, or, equivalently, stationarity of the ratio $E_{\rm turb}/E_{\rm g}$. In the energy equipartition and virial cases, we find $g = \sqrt{1/3} \approx 0.58$ and $g = \sqrt{1/6} \approx 0.41$, respectively, while in the stationary case we find $g = \langle v_{\rm rad} \rangle \mathcal{L}_{\rm d}/(4\pi\sqrt{3}\eta R v_{\rm g})$, where η is an efficiency factor in the energy dissipation rate, $\mathcal{L}_{\rm d}$ is the energy injection scale of the turbulence, and R is the core's radius.

Next, we perform adaptive mesh refinement simulations to follow the prestellar collapse of an isothermal, turbulent core, with an initial turbulent Mach number $\mathcal{M}_{\rm s} \approx 0.8$ at two different resolutions, to test for convergence. We also perform a non-turbulent control simulation. We find that the turbulent simulations collapse at the same rate as the non-turbulent run, so that the turbulence generation does not significantly slow down the collapse for these initial conditions during the prestellar stage. We also measure the ratio $h^2 \equiv \sigma_{\rm 1D}^2/\langle v_{\rm rad}^2 \rangle$ of the turbulent velocity dispersion to the total radial velocity dispersion, which we assume consists of the summation in quadrature of the gravitational and turbulent components. In the simulations, we find that this ratio first decreases, but later approaches a constant value, implying an approximation to near balance between the rates of energy injection from the collapse and of turbulence dissipation. We also find a value of $g \approx 0.395 \pm 0.035$, close to the "virial" value, and that the injection scale is $\mathcal{L}_{\rm d} \lesssim R$. Finally, we find that the "turbulent pressure" $\rho\sigma_{\rm 1D}^2$ scales with density as $\sim \rho^{1.64}$, thus having an apparently adiabatic polytropic exponent, in spite of the fact that the collapse is not delayed by the turbulence. We propose that both the apparently adiabatic polytropic exponent of the turbulent pressure and the nearly virial values of the turbulent velocity dispersion may be reconciled with the non-delayed collapse rate if the turbulence is dissipated as soon as it is generated, and conclude that the "heating" of turbulence by the collapse is extremely lossy,

rather than adiabatic.

I want to point out that this thesis is partially based on a paper recently submitted for review.

Acknowledgments

Al Instituto de Radioastronomía y Astrofísica de la UNAM campus Morelia y al personal que ahí labora (administración, cómputo y acervo) por brindar los medios y condiciones necesarios para mi desarrollo académico y profesional.

A la Dra. Aina Palau por brindarme el apoyo que me dio la oportunidad de iniciarme en el campo de la investigación científica.

Al Dr. Manuel Zamora por su recibimiento y asesoría en la revisión de los códigos que me permitieron la realización y posterior análisis de las simulaciones.

A mi asesor el Dr. Enrique Vázquez por su tiempo y paciencia para compartir sus conocimientos en las innumerables reuniones y pláticas, y por su acompañamiento que ha servido como motivación para continuar en este camino.

A los miembros del Comité Tutor la Dra. Jane Arthur, Dra. Adriana Gazol y Dra. Aina Palau por sus aportaciones e interés en el seguimiento a lo largo de la maestría.

A los miembros del sinodo Dr. Roberto Galván, Dr. Gilberto Gómez, Dra. Verónica Lora, Dr. Carlos Román y Dr. Manuel Zamora, por sus minuciosas revisiones y valiosos comentarios que llevaron a reflexiones y considerables mejoras al documento.

Contents

List of Figures

Chapter 1

Molecular Clouds

1.1 Motions in MCs: thermal and non-thermal

The Star Formation (SF) within the galaxies occurs in the densest regions of Giant Molecular Clouds (GMC). From the emission of certain molecules of dense gas, it is possible to know some physical parameters of the clouds like the temperature, the optical depth, the column density, and the cloud mass (see, e.g. Estalella and Anglada, 1999).

The first observation of Molecular Clouds (MCs) led us to the knowledge that they are associated with supersonic motions (Wilson et al., 1970). The linewidth allows us to estimate the total velocity dispersion (thermal and non-thermal). If we subtract the contribution due the temperature, we can obtain the non-thermal velocity dispersion, which corresponds to macroscopic motions inside the clouds.

To obtain the total component of the linewidth, we must take into account that the velocities are Gaussians and can be expressed as (see e.g. eq. (1) of Keto et al., 2008)

$$u_{tot}^2 = u_{nt}^2 + u_{th}^2 \tag{1.1}$$

The non-thermal motions can be defined as the macroscopic motions within the clouds, these can be produced by rotation, collapse, expansion, and turbulence.

1.2 Molecular Line Observations: Moments

The line emission or absorption of various molecular species provides abundant information about the kinematics of MCs. We can obtain spectra at multiple positions to cover the projected area of the object, this "spectroscopic mapping" generates three-dimensional data cubes of the line intensity at different position and frequencies or velocities known as position-position-

velocity (PPV) cubes.

The H_2 is a homonuclear molecule, and for this reason its dipole moment is zero, thus just can produce quadrupolar and superior order emission (very weak) at the temperature of MCs. For this, it is necessary to search for the emission of dust grains or other molecules that can be found in the same sites as H_2.

The next most abundant molecule in MCs after H_2 is ^{12}CO, but the high abundance of this tracer makes it often optically thick and cannot trace the properties of the turbulence in the deeper regions of a cloud. Studies of the properties of the turbulence within MCs often focus on less abundant isotopologues as ^{13}CO or C^{18}O. To trace the properties of the turbulence in MCs, different tracers are required.

Abundant kinematic information about MCs can be obtained from the moments of the line profiles in a PPV cube. These are obtained by treating the line profile at each position in the map as a distribution. The zeroeth moment, defined as

$$M_0 = \int I_\nu dv, \tag{1.2}$$

is the integrated intensity of the spectrum , where I_ν is the instensity of the emission at a certain frequency and v is the velocity channel. The first moment, defined as

$$M_1 = \frac{\int I_\nu v dv}{M_0}, \tag{1.3}$$

is the intensity-weighted mean radial velocity along the line of sight, or velocity centroid, and the second moment,

$$M_2 = \sqrt{\frac{\int I_\nu (v - M_1)^2 dv}{M_0}}, \tag{1.4}$$

is the intensity-weighted velocity dispersion. In summary, the moments of a molecular line map can give us information on the mean line-of-sight velocity and the linewidth of a spatially resolved object, and there are certain signatures that can give us an idea of whether the system is collapsing, expanding, or rotating.

1.3 Components of non-thermal Motions

When we observe non-thermal motions within MCs we are not able to distinguish between the different components as turbulence, infall, rotation or expansion, because the information comes to us along the line-of-sight. Even so, theoretically, we can decompose them in their different parts.

The two main large-scale motions within young MCs (which have not yet formed pre-stellar objects) are turbulence and collapse/accretion due to gravitational potential (see e.g. Lada et al., 1974; Bonazzola et al., 1987). These can be separated with the same method as we did for the thermal and non-thermal motions in Sec 1.1, a cuadratic sum

$$v_{nt}^2 = v_t^2 + v_g^2. \tag{1.5}$$

From this, we can estimate the amount of kinetic energy associated with each component, the turbulent energy and the infall energy. And as described above, we can add more components increasing the terms in the sum, but making more difficult to estimate the fraction of each component (as outflows/winds, etc.).

1.4 Collapse and Star Formation in MCs

1.4.1 Gravitational Collapse

For this analysis we assume a parcel of gas in the Interstellar Medium (ISM) in an equilibrium state between the thermal pressure gradient and its self-gravity, as originally done by Jeans (1902). To determine whether this equilibrium is a stable or this is an unstable state, we consider the evolution of a linear perturbation (see e.g. Ho and Cao, 1991, for the study of perturbation analysis).

For this it is necessary to use the fluid dynamics equations without viscosity, the Euler equations. First, the continuity equation is a statement of conservation of mass at any point

$$\frac{\partial \rho}{\partial t} + \nabla \cdot (\rho \mathbf{v}) = 0. \tag{1.6}$$

Integrating this equation over any small volume V surrounding the point $\mathbf{x}$ and applying the divergence theorem to the second term, this equation just says that the rate of change of $\int_{\mathrm{V}} \rho dV$, the total mass within V, is equal to $\oint_S \rho \mathbf{v} \cdot d\mathbf{S}$, the rate at which mass flows outward across the surface of V.

The second fundamental equation is the Euler equation, which is just the fluid equivalent of Newton's second law

$$\frac{\partial \mathbf{v}}{\partial t} + (\mathbf{v} \cdot \nabla)\, \mathbf{v} + \frac{1}{\rho} \nabla P + \nabla \varphi = 0. \tag{1.7}$$

Both the first and second term are the acceleration of the fluid. The third term is the pressure gradient, the force per unit volume on the fluid, divided by the density, the mass per unit volume. The last term is the force caused by the gravitational potential, where the gravitational

acceleration is $\mathbf{a} = -\nabla\varphi$ and the gravitational potential satisfies the Poisson's equation

$$\nabla^2\varphi = 4\pi G\rho, \tag{1.8}$$

where ρ is the density, $\mathbf{v}$ is the velocity, P is the pressure, and φ is the gravitational potential. Also, P and ρ are related by the ideal-gas equation of state

$$P = nkT. \tag{1.9}$$

We take the equilibrium solution given by $\rho = \rho_0 = cst$, $P = P_0 = cst$, and $v = 0$. The perturbation is denoted by the subscript 1 as $\rho = \rho_0 + \rho_1$, $P = P_0 + P_1$, $v = v_1$, and $\varphi = \varphi_0 + \varphi_1$. And the adiabatic sound speed can be approximated by

$$c_s^2 \equiv \left(\frac{\partial P}{\partial \rho}\right)_s \approx \frac{\gamma P_0}{\rho_0} \approx \frac{P_1}{\rho_1}, \tag{1.10}$$

making a first order expansion of the adiabatic law $P/P_0 = (\rho/\rho_0)^\gamma$. Then we introduce the perturbations into equations 1.6, 1.7 and 1.8. We obtain perturbed equations at first order of the form

$$\frac{\partial}{\partial t}\rho_1 + \rho_0\nabla\cdot\mathbf{v}_1 = 0 \tag{1.11}$$

$$\frac{\partial}{\partial t}\mathbf{v}_1 + \frac{c_s^2}{\rho_0}\nabla\rho_1 + \nabla\varphi_1 = 0 \tag{1.12}$$

$$\nabla^2\varphi_1 = 4\pi G\rho_1 \tag{1.13}$$

if we combine them, we obtain

$$\frac{\partial^2\rho_1}{\partial t^2} - c_s^2\nabla^2\rho_1 = 4\pi G\rho_0\rho_1 \tag{1.14}$$

which is a wave equation with an additional term due to self-gravity. Assuming a wave-like solution of the form

$$\rho_1(r,t) = A\rho_0 e^{i(\omega t - \mathbf{k}\cdot\mathbf{r})}, \tag{1.15}$$

the dispersion equation results as

$$\omega^2 = c_s^2 k - 4\pi G\rho_0. \tag{1.16}$$

From this we can see that ω can be real or imaginary, the real one has a wave behavior and the imaginary solution has an exponential behavior in time, the limit case is when

$$k > \left(\frac{4\pi G\rho_0}{c_s^2}\right)^{1/2} \tag{1.17}$$

and if we consider $k = 2\pi/\lambda$, we can obtain

$$\lambda < \left(\frac{\pi c_s^2}{G\rho_0}\right)^{1/2} \equiv L_{\rm J} \tag{1.18}$$

where $L_{\rm J}$ is defined as the Jeans length. Therefore, for a perturbation smaller than $L_{\rm J}$, the sonic crossing time ($\sim 1/(c_s k)$) is smaller than the free-fall time ($\sim 1/\sqrt{4\pi G\rho_0}$) and the perturbation can be restored before the collapse. In the other case, for λ larger than $L_{\rm J}$, the opposite happens.

The mass corresponding to $L_{\rm J}$ can be estimated by assuming a sphere of uniform density with diameter $L_{\rm J}$, to obtain the maximum mass that can be supported by thermal pressure against its self-gravity, known as the Jeans mass

$$M_{\rm J} \equiv \frac{\pi^{5/2}}{6}\frac{c_s^3}{G^{3/2}\rho_0^{1/2}} \propto \rho_0^{-1/2}. \tag{1.19}$$

We are simplifying this analysis by considering just the thermal pressure, the self-gravity, and spherical geometry. In conclusion, if the mass within a region is larger than the Jeans mass, the region proceeds to collapse.

1.4.2 Star Formation

MCs are the regions of Star Formation in the Galaxy. This is due to their low temperature and high density ($T \sim 10-20$ K, $n \sim 10^2-10^6$ cm^{-3}, Ferrière, 2001) which causes the Jeans mass to be low ($M_{\rm J} \sim 3-150\ M_\odot$). The MCs have density structures that are hierarchically organized. At a larger scale we have the Giant Molecular Clouds (GMC) with sizes of tens of parsecs and densities of $n \sim 10^3$ cm^{-3}, passing through clumps, filaments, unto small dense cores with sizes of ~ 0.1 pc and densities of $n \sim 10^5$ cm^{-3} (Larson, 1981, shown in Fig. 1.1).

A pre-stellar core is a density structure generated by turbulent shock compressions and local reduction in Jeans mass (Mac Low and Klessen, 2004). As we saw in the last section (Sec. 1.4.1), if the mass within a volume is enough, then proceeds to collapse; otherwise, reexpands. The density and velocity profiles of collapsing cores display characteristic features. In the inner part the density is flat and the velocity increases linearly with the radius, at the envelope the density decreases as r^{-2} and the velocity becomes constant (see e.g. Whitworth and Summers, 1985; Naranjo-Romero et al., 2015). Also this structures often exhibit trans- or even sub-sonic non-thermal linewidths (Jijina et al., 1999; Tafalla et al., 2004).

The general belief since the 1980's (standard model, Shu et al., 1987) was that prestellar cores in low-mass-star-forming regions evolve quasi-statically in magnetically subcritical clouds, when the magnetic energy $\mathcal{M}$ is larger than the gravitational energy W (see Sec. 2.2.2 for further

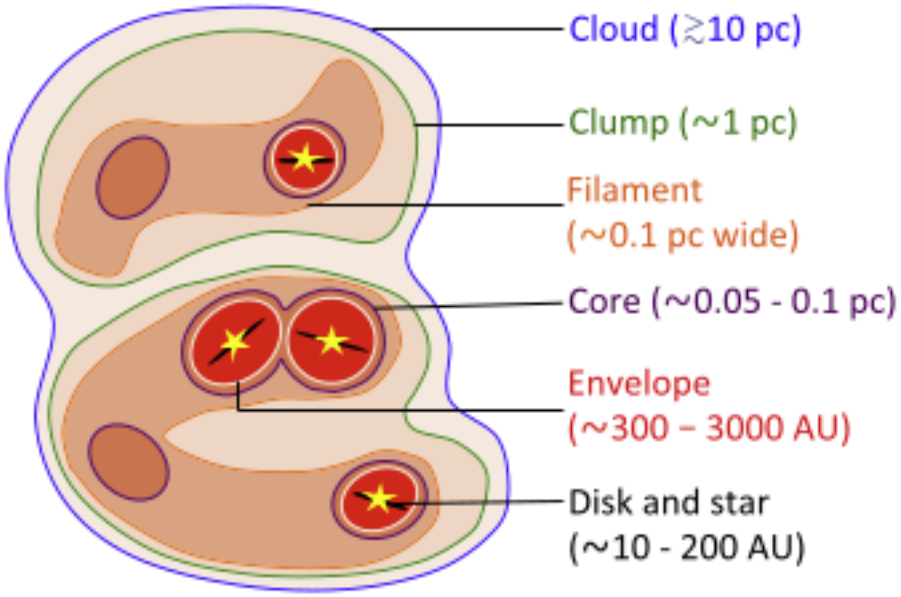

Figure 1.1: Cartoon of the hierarchical stucture of a MC that shows the different density structures (not scaled) as clumps, filaments, cores, etc. Taken from Pokhrel et al. (2018).

explanation). The fact that most cloud cores are magnetically supercritical ($W > \mathcal{M}$, Crutcher et al., 1999) motivated a shift towards considering supersonic turbulence as one of the primary agents supporting the clouds and regulating the stellar birth to set the Star Formation Rate (SFR) and Star Formation Efficiency (SFE) observed, for example, in the Galaxy (2 $M_\odot$ yr^{-1} and $\sim 5\%$, respectively, Chomiuk and Povich, 2011; Gao and Solomon, 2004).

For star cluster formation it is believed that the gravitational energy must dominate the energy budget of massive cloud cores, meaning that the entire region is contracting (Klessen, 2011). The supersonic turbulence produces a high degree of internal sub-structure with large density contrasts (Klessen and Glover, 2016). Some of these density fluctuations are gravitationally unstable and have shorter free-fall times than the entire cloud as the free-fall time scales with the density as $t_{\rm ff} \propto \rho^{-1/2}$ (Vázquez-Semadeni et al., 2019).

The densest regions collapse before other regions. These are statistically located in the deepest gravitational potential well (mass segregation, Elmegreen et al., 2006) and can accrete more mass than those that form later and are located at the external parts of the core, and can only primarly accrete from its local potential well (competitive accretion, Bonnell et al., 2001, as shown in Fig. 1.2). Once the massive stars cease to accrete and begin to ionize their environment, they create bubbles of hot ionized gas which expand and enclose the stellar cluster. The global effect is that the MCs disperse and no new stars can form and stellar birth comes to an end. But it was also found that locally, this ionized and shocked fronts from stellar feedback can sweep and collect the material to enhance sequential star formation (Elmegreen and Lada,

1977).

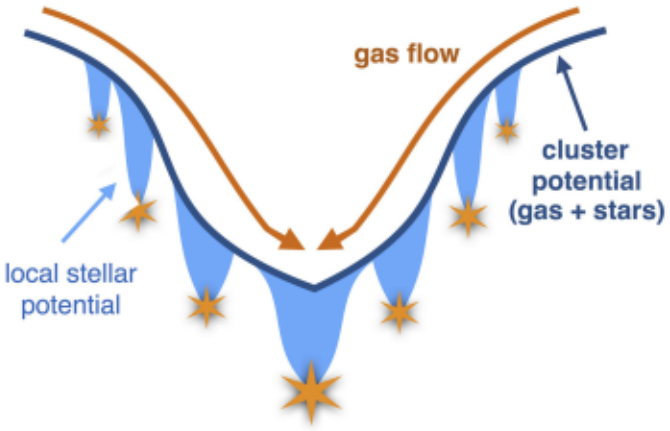

Figure 1.2: Cartoon of Competitive Accretion showing a larger accretion rate for the (proto) stars located in the deepest potential well. Taken from Wright (2015).

Chapter 2

Turbulence in MCs

2.1 Turbulence

Turbulence is a regime of flow disordered in space and time that occurs in fluids when the ratio of the magnitude of the advection term (momentum transport) is sufficiently larger than the viscous term (damping force, see e.g. Ch. 1 of Lesieur, 2008). This ratio is known as the Reynolds number

$$Re \equiv \frac{|\mathbf{u} \cdot \nabla \mathbf{u}|}{|\nu \nabla^2 \mathbf{u}|}. \tag{2.1}$$

A turbulent flow is characterized by the following features:

- The system is unpredictable and chaotic, so that is impossible to make an exact prediction of its evolution.
- It involves a wide range of spatial scales, described by degrees of freedom or modes of a Fourier decomposition.
- These modes are able to nonlinearly exchange energy. This implies that the flow exhibits the property of "mixing", so that the values of its physical properties (density, velocity, temperature, magnetic field strength) are transported ("advected") by the fluid motions.

2.1.1 Turbulence Scales and Energy Spectrum

Kolmogorov (1941) developed a theory for homogeneous incompressible turbulence based on the following assumptions:

- A very large range of scales are active in the flow.
- Energy is injected at large scales and dissipated at small scales.

- Energy can be transferred among the scales, or modes.
- The system is in a stationary state.

Then, considering that the energy transfer rate for eddies (vortices) of scale size ℓ can be written as $\dot{\varepsilon} \sim u_\ell^2/\tau_\ell$, where u_ℓ is the characteristic velocity of the eddy, and $\tau_\ell = \ell/u_\ell$ is the eddy turnover time at scale ℓ. Thus, the velocity can be expressed as

$$u_\ell = (\dot{\varepsilon}\ell)^{1/3}. \tag{2.2}$$

Now, we can relate the characteristic velocity at scale ℓ with the rms specific kinetic energy given by the energy spectrum

$$u^2 = 2\int_{2\pi/\ell}^{\infty} E(k)dk, \tag{2.3}$$

assuming that the total energy at scale ℓ is the energy contained within that scale and lower scales. Assuming a power-law dependence on wavenumber for the spectrum of the form $E(k) \propto k^{-n}$, and substituiting the scaling relation 2.2, we obtain

$$\ell^{2/3} \propto \int_{2\pi/\ell}^{\infty} k^{-n}dk \propto \ell^{n-1}, \tag{2.4}$$

resulting in $n = 5/3$.

This theory involves fundamental concepts: a $k^{-5/3}$ energy spectrum, an energy cascade from large to small scales, and the highest amount of energy is contained in the largest scales (shown in fig. 2.1). It is important to note that the MCs are a compressible fluid so, turbulence in MCs is not necessarily characterized by these properties and inverse cascades can occur.

2.1.2 Injection and Dissiaption of Turbulence

To compute the total rate of change of the specific kinetic energy in a volume V of the flow, we take the dot product of the momentum equation per-unit-mass with the velocity vector to obtain

$$\mathbf{u}\frac{d\mathbf{u}}{dt} = -\mathbf{u}\frac{\nabla P}{\rho} + \frac{\mu}{\rho}\mathbf{u}\cdot\nabla^2\mathbf{u} + \mathbf{u}\cdot\nabla\varphi, \tag{2.5}$$

taking the gravitational potential as the generator of the driving force. To bring the velocities inside the spatial derivatives, this equation can be rewritten as

$$\frac{1}{2}\frac{d\mathbf{u}^2}{dt} = -\frac{1}{\rho}\nabla\cdot(\mathbf{u}P) + \frac{\mu}{\rho}\mathbf{u}\cdot\nabla^2\mathbf{u} + \mathbf{u}\cdot\nabla\varphi. \tag{2.6}$$

Then we integrate over all space and apply Gauss' theorem, to get

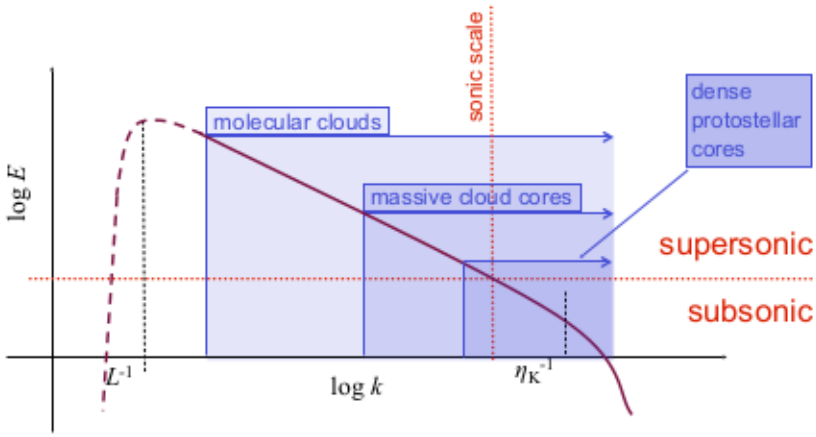

Figure 2.1: Cartoon of the turbulent energy spectrum. The energy is injected a large scales and dissipated at small scales developing a $-5/3$ slope among a wide range of spatial scales. Taken from Klessen (2011).

$$\frac{dE_{\rm tot}}{dt} \equiv \frac{1}{2}\frac{d\mathbf{u}^2}{dt} = -\frac{1}{\rho}\oint P\mathbf{u}\cdot d\mathbf{S} + \int_V \frac{\mu}{\rho}\mathbf{u}\cdot\nabla^2\mathbf{u}dV + \int_V \mathbf{u}\cdot\nabla\varphi dV, \tag{2.7}$$

where S is the surface enclosing the volume V, and $E_{\rm tot}$ is the total kinetic energy per unit mass in the volume. Letting $V \to \infty$ and assuming that the pressure vanish at infinity, the surface term vanish and we get

$$\frac{dE_{\rm tot}}{dt} = \int_V \nu\mathbf{u}\cdot\nabla^2\mathbf{u}dV + \int_V \mathbf{u}\cdot\nabla\varphi dV, \tag{2.8}$$

where $\nu = \mu/\rho$ is the kinematic viscosity. This implies that the total rate of change of the specific energy is given by the injection from the work done by gravity minus the dissipation caused by viscosity. If we now consider a stationary regime, in which the kinetic energy remains constant, the left hand side of the eq. 2.8 vanishes, and we can write

$$\int_V \mathbf{u}\cdot\nabla\varphi dV = \int_V \nu\mathbf{u}\cdot\nabla^2\mathbf{u}dV, \tag{2.9}$$

which means that, in a stationary regime, the kinetic energy injected by the self-gravity must be dissipated by viscosity. Also we can see that the dissipation rate depends only on the injection rate. This reflects the well-known fact that the dissipation rate in fully developed turbulence does not depend on the specific value of the viscosity coefficient, but only on the injection rate,

because the former rate adjusts itself to the latter by occurring on scales sufficiently small for the viscous term to be important.

2.2 Virial Theorem

The Virial Theorem (VT) is an expression of the energy balance of a certain region in a fluid, representing the change in the kinetic energy and mass distribution within the parcel as a consequence of the work done by all the forces acting in the region. It is obtained from the momentum equation,

$$\frac{d\mathbf{u}}{dt} = -\frac{\nabla P}{\rho} - \nabla\varphi + \frac{1}{4\pi\rho}\left(\nabla \times \mathbf{B}\right) \times \mathbf{B}, \tag{2.10}$$

where $\mathbf{u}$ is the velocity, P is the pressure, ρ is the density, φ is the gravitational potential, and $\mathbf{B}$ is the magnetic field, multipliying it by the position vector $\mathbf{x}$, and integrating over a fixed volume V

$$\int_V \rho\mathbf{x} \cdot \frac{d\mathbf{u}}{dt} dV = -\int_V \mathbf{x} \cdot \nabla P dV - \int_V \rho\mathbf{x} \cdot \nabla\varphi dV + \frac{1}{4\pi}\int_V \mathbf{x} \cdot (\nabla \times \mathbf{B}) \times \mathbf{B} dV. \tag{2.11}$$

Considering that, $d/dt = \partial/\partial t + \mathbf{u} \cdot \nabla$, we can rewrite the left hand side as

$$\int_V \rho\mathbf{x} \cdot \frac{d\mathbf{u}}{dt} dV = \frac{1}{2}\int \frac{d^2\mathbf{x}^2}{dt^2} dm - \int_V \rho\mathbf{u}^2 dV, \tag{2.12}$$

the first term is similar to the inertia tensor, I, which describes the distribution of the mass in the space, and the second term is twice the kinetic energy. Following with the right hand side, we can rewrite the gravitational term using the Poisson's equation

$$W = \int_V \rho(\mathbf{x})\mathbf{x} \cdot \nabla\varphi dV = -G\int_V \int_\infty \frac{\rho(\mathbf{x})\rho(\mathbf{x}')\mathbf{x} \cdot (\mathbf{x} - \mathbf{x}')}{|\mathbf{x} - \mathbf{x}'|^3} dV' dV. \tag{2.13}$$

Noting that the integrand is nearly symmetric with respect to the primed and unprimed variables, we can replace $\mathbf{x}$ by $(\mathbf{x} - \mathbf{x}')/2$ and write

$$W = -\frac{1}{2}G\int_V \int_\infty \frac{\rho(\mathbf{x})\rho(\mathbf{x}')}{|\mathbf{x} - \mathbf{x}'|} dV dV'. \tag{2.14}$$

Then, the thermal and magnetic terms can be dealt using the Gauss's divergence theorem and the fact that $\nabla \cdot \mathbf{x} = 3$ and that $\partial x_i/\partial x_j = \delta_{ij}$. Also, for the magnetic term, is better to work

with the Maxwell's magnetic stress tensor $\mathbf{T} \equiv T_{ij} \equiv B_i B_j/4\pi - |\mathbf{B}|^2\delta_{ij}/8\pi$. Thus we obtain

$$\begin{aligned}\frac{1}{2}\int \frac{d^2\mathbf{x}^2}{dt^2}\rho dV - \int_V \rho \mathbf{u}^2 dV = &\left(3\int P dV - \oint_S P\mathbf{x}\cdot d\mathbf{S}\right) \\ &+ \left(\frac{1}{8\pi}\int B^2 dV + \oint_S \mathbf{x}\cdot\mathbf{T}\cdot d\mathbf{S}\right) \\ &- \frac{1}{2}G\int_V\int_\infty \frac{\rho(\mathbf{x})\rho(\mathbf{x}')}{|\mathbf{x}-\mathbf{x}'|}dV dV'.\end{aligned} \tag{2.15}$$

This equation can be written as

$$\frac{1}{2}\int \frac{d^2\mathbf{x}^2}{dt^2}\rho dV - 2K = \left(2U - \oint_S P\mathbf{x}\cdot d\mathbf{S}\right) + \left(\mathcal{M} + \oint_S \mathbf{x}\cdot\mathbf{T}\cdot d\mathbf{S}\right) + W, \tag{2.16}$$

where S is the surface enclosing V, and K, U $\mathcal{M}$, W are the kinetic, internal, magnetic and gravitational energies, respectively, and $\mathbf{T}$ is the Maxwell stress tensor. The system is said to be in virial equilibrium if this is equal to zero.

2.2.1 Hydrostatic Equilibrium and Turbulent Support

Taking the VT for an unmagnetized cloud at rest, so that $\mathbf{B} = \mathbf{u} = 0$, neglecting external pressure, the virial equilibrium condition reduces to

$$W = -2U, \tag{2.17}$$

where W is the gravitational energy and U is the internal energy. This implies hydrostatic equilibrium between the pressure gradient and the gravitational energy. If we also include a turbulent velocity field we obtain

$$W = -2(U + K), \tag{2.18}$$

where K is the kinetic energy of the turbulent field. We can extrapolate the hydrostatic equilibrium with this case assuming that the velocity field is displayed by micro turbulence (small-scale turbulence that does not destroy density structures) and this additional term can provide additional support against gravity, which supplements that provided by the thermal pressure gradient.

In the case when the external pressure is not negligible we can obtain

$$P_{\text{ext}} = \frac{2U + W}{3V}, \tag{2.19}$$

where P_{ext} is the external pressure, and V is the volume of the region.

2.2.2 Magnetic Support

If we assume now a uniform-density, isolated spherical cloud of fixed mass M, radius R, permeated by a uniform magnetic field $\mathbf{B} = B_0\hat{\mathbf{e}}_x$ inside and a vanishing field outside, and with $\mathbf{u} = P = 0$. In this case, the gravitational energy can be computed as

$$W = -G\int \frac{M(r)}{r} dM(r) = -\frac{3}{5}\frac{GM^2}{R}, \tag{2.20}$$

where $M(r)$ is the mass interior to radius r. The magnetic energy is

$$\mathcal{M} = \frac{B_0^2 R^3}{6} \equiv \frac{\phi^2}{6\pi^2 R}, \tag{2.21}$$

where ϕ is the magnetic flux, which, according to the flux-freezing condition, is conserved in the absence of magnetic dissipation. Since ϕ is constant, both W and $\mathcal{M}$ scale as R^{-1} upon contraction, and the ratio $W/\mathcal{M}$ is constant. This implies that there is a critical mass-to-flux ratio

$$\left(\frac{M}{\phi}\right)_{\rm crit} \equiv \left(\frac{5}{18}\right)^{1/2}\left(\frac{1}{\pi^2 G}\right)^{1/2}, \tag{2.22}$$

below which a cloud cannot collapse gravitationally since, for masses smaller than that, the magnetic energy $\mathcal{M}$ is larger than the gravitational energy W (Mestel and Spitzer, 1956). If this ratio for an specific cloud is larger than the critical value, the cloud is said to be magnetically supercritical, and it cannot be supported by the magnetic field. Otherwise, it is called magnetically subcritical.

2.3 Support Against Gravity?

Shortly after supersonic motions within MCs were first observed (Wilson et al., 1970), Goldreich and Kwan (1974) proposed global gravitational contraction, and these velocities could be explained as being produced by the cloud's own gravitational potential. However, Zuckerman and Evans (1974) argued that a MC dominated by global collapse should exhibit a systematic Doppler shift between emission lines coming from the back of the cloud and absorption lines produced at its front part, due to the velocity difference between these different parts of the cloud (see Fig. 2.2). Since such shifts were not observed at the time, they instead proposed that these supersonic linewidths could be primarily dominated by local motions, therefore constituting micro-turbulence.

The turbulent support model is derived from the fact that the clouds exhibit a near equipartition state between the non-thermal kinetic and the gravitational energies (Larson, 1981; Heyer

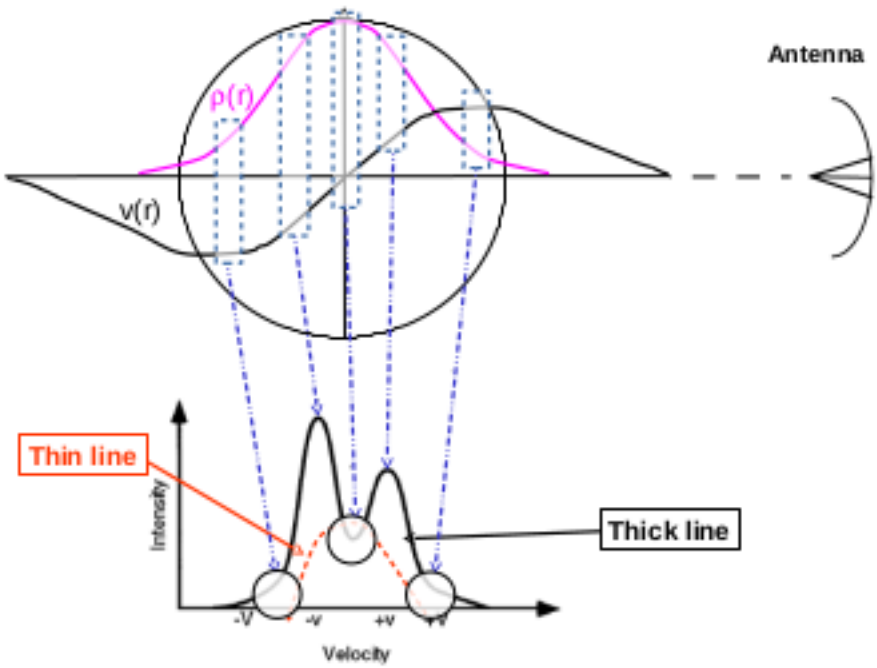

Figure 2.2: Schematic figure of the signature of collapse line profile, generated escencially by the density and velocity profiles. Taken from Loughnane et al. (2018).

et al., 2009). This is often intrerpreted as an evidence of virial equilibrium between turbulence and self-gravity.

As seen before, the turbulence contains a large number of excited scales and this property implies a modern version of turbulent support in which turbulence plays a dual role (Vázquez-Semadeni et al., 2003; Mac Low and Klessen, 2004): For a certain density structure of a typical size scale ℓ, the turbulent velocity modes of size scale ℓ_t smaller than the density structure $\ell_t < \ell$, are believed to provide support against self-gravity through their turbulent pressure $\rho\sigma_t^2$. But turbulent velocity modes larger than the density structure ($\ell_t > \ell$), are believed to form or destroy these density fluctuations through shocks and shearing, respectively.

In this model, the clouds are thought to be strongly supersonic turbulent so that the turbulence is capable of creating turbulent density fluctuations, but also prevent the global collapse with the kinetic energy associated. On the other hand, the local compressions caused by the turbulence undergo a decrease of the Jeans mass and proceed to collapse if the local Jeans mass becomes smaller than the clump/core mass.

2.4 Turbulence Driven by Gravitational Collapse

As discussed in Sec. 2.1.2, an important property of turbulence is that it is a highly dissipative phenomenon, and numerical simulations show that it dissipates roughly in a crossing time (Stone et al., 1998; Mac Low, 1999; Avila-Reese and Vázquez-Semadeni, 2001; Lemaster and Stone, 2009), so that maintaining the observed kinetic energy in MCs requires a continuous driving mechanism. There is a large number of physical processes that could drive the observed turbulence in MCs, such as:

1. Magnetorotational instabilities that generate Maxwell stresses that transfer energy from shear into turbulent motions (Balbus and Hawley, 1991).

2. Stellar feedback processes that act as sources of turbulence. From their birth to their death, stars interact with their environment through jets and outflows (Lada, 1985), stellar winds (Norman and Silk, 1980), ionizing radiation (McKee, 1989) and supernova explosions (McKee and Ostriker, 1977; Spitzer, 1978).

3. Accretion. This is a universal process driven by gravity, implying that all structures in the Interstellar Medium appear to accrete from their parent structures, transferring kinetic energy from the parent to the daughter structures (Field et al., 2008; Vázquez-Semadeni et al., 2009; Klessen and Hennebelle, 2010; Vázquez-Semadeni et al., 2019). Klessen and Hennebelle (2010) have shown that only about 1-10% of the infall energy from the parent scale is needed to explain the turbulent energy in the daughter scale.

Also, there is a "heating" mechanism that results from the gravitational contraction of a turbulent fluid (Robertson and Goldreich, 2012), in which the turbulent eddies are amplified as a consequence of gravitational contraction. This turbulence reaches a level similar to equipartition (Robertson and Goldreich, 2012) or virialization, and it is suggested that this is enough to delay the collapse (Murray and Chang, 2015; Li, 2018; Xu and Lazarian, 2020).

We investigate the gravitational contraction mechanism in detail both analytically and numerically. We start by writing expressions for the expected levels of turbulence generated during gravitational collapse under the conditions of energy equipartition between kinetic turbulent energy and gravitational energy, virial equilibrium, and equality of the injection and dissipation rates. We then perform numerical simulations and measure the corresponding energies, to determine the situation that occurs in the simulations.

Chapter 3

Analytical Estimates

3.1 Definitions

In this section, we investigate the generation of turbulence during spherical gravitational collapse analytically (Murray and Chang, 2015; Li, 2018; Xu and Lazarian, 2020), assuming that the interplay between injection and dissipation rates achieves a stationary regime. Specifically, we present an analytical estimation of the expected value of the ratio $g \equiv \sigma_{\rm 1D}/v_{\rm g}$ of the one-dimensional turbulent velocity dispersion, $\sigma_{\rm 1D}$, to the gravitational velocity given by

$$v_{\rm g} = \sqrt{\frac{2\beta GM}{R}}, \tag{3.1}$$

of a spherical cloud of fixed mass M and radius R. Here, β is a geometrical factor of order unity (for a sphere of uniform density $\beta = 5/3$). We perform the estimate under two alternative reasonable assumptions: i) that the system approaches equipartition or virial balance between the gravitational ($E_{\rm g}$) and the turbulent kinetic energy ($E_{\rm turb}$), or ii) that the system attains an arbitrary, yet self-consistent, stationary value of the ratio of the two energies, where the energy injection rate balances the dissipation rate.

We start by decomposing the total velocity in spherical coordinates into its radial and tangential components, $v_{\rm rad}$ and $v_{\rm tan}$, where we define

$$\langle v_{\rm tan}^2 \rangle_{\rm 1D} = \frac{\langle v_\theta^2 \rangle + \langle v_\varphi^2 \rangle}{2} \equiv \sigma_{\rm 1D}^2. \tag{3.2}$$

The last equality states that we identify $\langle v_{\rm tan}^2 \rangle_{\rm 1D}^{1/2}$ with the one-dimensional velocity dispersion of the turbulence, averaging the variance of the angular components for better precision. For sim-

plicity, in what follows we drop the subindex $1D$ from $\langle v_{\rm tan}^2\rangle_{\rm 1D}^{1/2}$. [a] We use this definition instead of the usual definition $\sigma_{\rm 1D}^2 = \left(\langle v_{\rm rad}^2\rangle + \langle v_\varphi^2\rangle + \langle v_\theta^2\rangle\right)/3$, which implies isotropy in the turbulence, because $v_{\rm rad}$ contains a possibly dominant contribution from infall rather than from turbulence just after the initial times when the collapse begins to be important. On the other hand, note that $\langle v_{\rm rad}^2\rangle^{1/2}$ is expected to contain contributions from both the turbulent fluctuations and the infall speed, so that

$$\langle v_{\rm rad}^2\rangle = \sigma_{\rm 1D}^2 + v_{\rm g}^2. \tag{3.3}$$

We thus define the ratio

$$f^2 \equiv \frac{\langle v_{\rm rad}^2\rangle}{v_{\rm g}^2} \tag{3.4}$$

as a measure of the excess kinetic energy in the collapse due to the turbulence.

The main quantity we are interested in is the ratio of the one-dimensional turbulent velocity dispersion $\sigma_{\rm 1D}$ to the gravitational speed,

$$g^2 \equiv \frac{\sigma_{\rm 1D}^2}{v_{\rm g}^2}, \tag{3.5}$$

which determines the fraction of energy going from the gravitational contraction to the turbulent motions.

From eqs. (3.4) and (3.5), we also obtain

$$\frac{\sigma_{\rm 1D}^2}{\langle v_{\rm rad}^2\rangle} = \frac{g^2}{f^2} \equiv h^2, \tag{3.6}$$

which is another quantity we will measure directly from our numerical simulations, in order to obtain g.

3.2 Energy equipartition and virialization

We now estimate the value of the ratio g in the case that the infall kinetic energy attains equipartition or virial equilibrium with the gravitational energy. First, assuming that the turbulence is isotropic, we write the turbulent kinetic energy as

$$E_{\rm turb} \approx \frac{1}{2}\sigma_{\rm 3D}^2 M = \frac{3}{2}\sigma_{\rm 1D}^2 M. \tag{3.7}$$

[a] Note that, strictly speaking, the total tangential velocity dispersion is $\langle v_{\rm tan}^2\rangle^{1/2} = \langle v_\theta^2\rangle + \langle v_\varphi^2\rangle$, but here we directly identify this symbol with the one-dimensional dispersion in the tangential directions.

Inserting eq. (3.5) in (3.7), we thus find

$$E_{\rm turb} = \frac{3}{2} g^2 v_{\rm g}^2 M. \tag{3.8}$$

On the other hand, we have, for the gravitational energy,

$$E_{\rm g} = -\frac{\beta G M^2}{R} = -\frac{1}{2} v_{\rm g}^2 M. \tag{3.9}$$

using the definition for the gravitational velocity as in eq. (3.1). Therefore, in the case of equipartition, where $E_{\rm turb} = |E_{\rm g}|$, we find

$$g_{\rm eq} = \sqrt{\frac{1}{3}} \approx 0.58. \tag{3.10}$$

where we have denoted by $g_{\rm eq}$ the value of g corresponding to equipartition.

In the case of virial equilibrium, in which $2E_{\rm turb} = |E_{\rm g}|$, we obtain

$$g_{\rm vir} = \sqrt{\frac{1}{6}} \approx 0.41. \tag{3.11}$$

3.3 Self-consistent stationary regime

We now consider the possibly more realistic situation that the system adjusts itself to a stationary regime in which the rate of energy injection into the turbulence due to the release of gravitational energy balances the dissipation rate of the turbulence by viscosity. We write this condition as

$$\dot{E}_{\rm turb} = \dot{E}_{\rm g}. \tag{3.12}$$

This condition has been investigated by Li (2018), although this author made some *ad hoc* assumptions about the parameters entering the above rates, while instead here we leave them open, to be determined from the results of our numerical simulations.

To compute the energy injection rate from the release of gravitational energy, we differentiate the gravitational energy given by eqs. (3.1) and (3.9)

$$\begin{aligned} \dot{E}_{\rm g} &= \frac{d}{dt}\left(-\frac{\beta G M^2}{R}\right) \approx \frac{\beta G M^2 \langle v_{\rm rad}\rangle}{R^2} \\ &= -\frac{\langle v_{\rm rad}\rangle}{v_{\rm g}} \left(\frac{2|E_{\rm g}|^3}{M R^2}\right)^{1/2}, \end{aligned} \tag{3.13}$$

where in the first equality we have written $\dot{R} \approx \langle v_{\rm rad}\rangle$, with the average computed over a

spherical shell of radius R (implying that the average can be a function of R) , and in the second equality we have introduced the velocity $v_{\rm g}$ as defined by eq. (3.1). Note that the ratio $\langle v_{\rm rad}\rangle/v_{\rm g}$ is not the same as the ratio f defined in eq. (3.4), which involves the variance of $v_{\rm rad}$, while $\langle v_{\rm rad}\rangle/v_{\rm g}$ involves the mean value of $v_{\rm rad}$.

On the other hand, for the kinetic energy dissipation rate, we use the expression provided by Mac Low (1999, hereafter, ML99):

$$\dot{E}_{\rm turb} = -\frac{2\pi\eta_{\rm ML} M\sigma_{\rm 3D}^3}{\mathcal{L}_{\rm d}}, \tag{3.14}$$

where M is the mass of the system, $\mathcal{L}_{\rm d}$ is the energy-injection scale of the turbulence, and $\eta_{\rm ML} \approx 0.21/\pi \approx 0.067$ is a constant he determined from numerical simulation of driven isothermal turbulence in a periodic box. We refer in general to the proportionality constant, η, as the *dissipation efficiency*, and allow for the possibility that it differs in our problem from the value found by ML99, $\eta_{\rm ML}$, due to the different nature of the energy injection (using Fourier driving), physical problem (stationary driven turbulence) and injection scale (at the largest scales) used by ML99, so we drop the subindex "ML". Thus, inserting eq. (3.7) into eq. (3.14), we obtain

$$\dot{E}_{\rm turb} = -2\pi\eta\left(\frac{2^3 E_{\rm turb}^3}{M\mathcal{L}_{\rm d}^2}\right)^{1/2}. \tag{3.15}$$

We can now compute the derivative of the ratio of the two energies (in absolute value, since we equate the turbulent dissipation rate to the gravitational injection rate), and set it to zero to demand stationarity:

$$\frac{d}{dt}\left(\frac{E_{\rm turb}}{|E_{\rm g}|}\right) = \frac{|E_{\rm g}||\dot{E}_{\rm turb}| - |E_{\rm turb}||\dot{E}_{\rm g}|}{E_{\rm g}^2} = 0.$$

This condition is satisfied when

$$4\pi\eta\frac{|E_{\rm g}|E_{\rm turb}^{3/2}}{\mathcal{L}_{\rm d}} = \frac{\langle v_{\rm rad}\rangle}{v_{\rm g}}\frac{E_{\rm turb}|E_{\rm g}|^{3/2}}{R},$$

which implies

$$E_{\rm turb} = \left(\frac{1}{4\pi\eta}\frac{\langle v_{\rm rad}\rangle}{v_{\rm g}}\frac{\mathcal{L}_{\rm d}}{R}\right)^2 |E_{\rm g}|. \tag{3.16}$$

This implies that the velocity ratio g in the stationary regime is

$$g_{\rm st} = \frac{1}{4\pi\sqrt{3}}\frac{\langle v_{\rm rad}\rangle}{v_{\rm g}}\frac{\mathcal{L}_{\rm d}}{\eta R}. \tag{3.17}$$

If we adopt the value of η found by ML99, we find

$$g_{\mathrm{st,ML}} \approx 0.687 \frac{\langle v_{\mathrm{rad}} \rangle}{v_{\mathrm{g}}} \frac{\mathcal{L}_{\mathrm{d}}}{R}. \tag{3.18}$$

In the next section, we will estimate the ratio $\langle v_{\mathrm{rad}} \rangle / v_{\mathrm{g}}$ from our numerical simulations. This will allow the calculation of the ratio of the driving scale to the core's radius, provided we assume $\eta = \eta_{\mathrm{ML}}$. Otherwise, eq. (3.17) shows that there is an unresolvable degeneracy between the dissipation efficiency and the ratio of the driving scale to the radius of the sphere, which in our case is not known. It can be assumed that it is the radius or the diameter of the core (as done by Li, 2018), but our numerical experiments will not allow us to resolve this degeneracy.

Chapter 4

Numerical Simulations

We use the Eulerian adaptive mesh refinement (AMR) code FLASH2.5 (Fryxell et al., 2000) to perform two 3D numerical simulations of the gravitational collapse of a dense core in presence of a turbulent velocity field, to determine the transfer of energy from the gravitational to the turbulent motions. These two turbulent simulations differ in the maximum resolution and refinement criterion, to test for convergence. We also consider a reference non-turbulent simulation.

We consider a numerical box filled with isothermal molecular gas, so that the simulation is scale-free. The sound speed and the mean density are set so that the box size is $L_{\rm b} \approx 2.48 L_{\rm J}$, where $L_{\rm J} = (\pi c_{\rm s}^2 / G\langle\rho\rangle)^{1/2}$ is the Jeans length, and $\langle\rho\rangle$ is the mean density. The boundary conditions are periodic for the hydrodynamics, and isolated for the self-gravity.

The simulations are initiated with a uniform density ρ_0, on top of which a spherically symmetric Gaussian density profile, centered at the center of the numerical box, is added. This Gaussian profile has a peak value of $\rho_{\rm max} = 2.5\rho_0$ and a width $\sigma_\rho = 0.25 L_{\rm b}$. Therefore, the maximum density within the box is $\rho_{\rm max} = 3.5\rho_0$. The mean density is $\langle\rho\rangle = 1.535\rho_0$. The physical values for this variables are $n_0 = 4.86 \times 10^5$ part cm^{-3}, $c_s = 0.21$ km s^{-1}, and L$_{\rm b}$ = 0.1 pc.

We start the simulations with a turbulent driver to stir the gas, using the prescription of Price and Federrath (2010), over roughly one crossing time. We then turn off the driving and turn on self-gravity, so that the gas begins to collapse, and the turbulence drains energy from the collapse motions. The initial turbulent velocity dispersion is $\sigma_{\rm 3D} \approx 0.8 c_{\rm s}$. The energy is injected in a range of scales between $L_{\rm b}/8$ and $L_{\rm b}/32$, so that the fluctuations fit within the Gaussian peak. The driving is fully solenoidal. We do not include magnetic fields in our simulation. Table 4.1 gives a summary of the parameters of the simulations. Figure 4.1 shows one cross section of the turbulent core at time $t \approx t_{\rm ff}$. Note that, as pointed out by Larson (1969), the actual collapse time of the simulation is longer than $t_{\rm ff}$ because at the early stages of the collapse, the

Table 4.1: Run parameters.

Run	Effective refinement (pc)	Cells / Jeans length	σ_{3D}/c_s
no turb	9.76×10^{-5}	12	0.0
turb 08	9.76×10^{-5}	12	0.8
turb 10	2.44×10^{-5}	24	0.8

thermal pressure gradient is not negligible.

We note that, according to the standard Jeans criterion (Truelove et al., 1997), the local Jeans length should be resolved by at least 4 cells. Actually, we resolve it with a significantly larger number of cells, in order to avoid excessive dissipation within the core. This is because, as is well known (e.g., Whitworth and Summers, 1985; Keto and Caselli, 2010), the inner part of a prestellar core, in which the density is roughly flat and the infall speed increases linearly with radius, has a radius of roughly one Jeans length of the central density. Therefore, the resolution applied to the Jeans length is equivalent to that applied to the central part of the core, which we want to be sufficiently resolved as to avoid excessive numerical dissipation of the turbulence within the core. We thus use 12 cells per Jeans length in the low-resolution run and 24 in the high-resolution one.

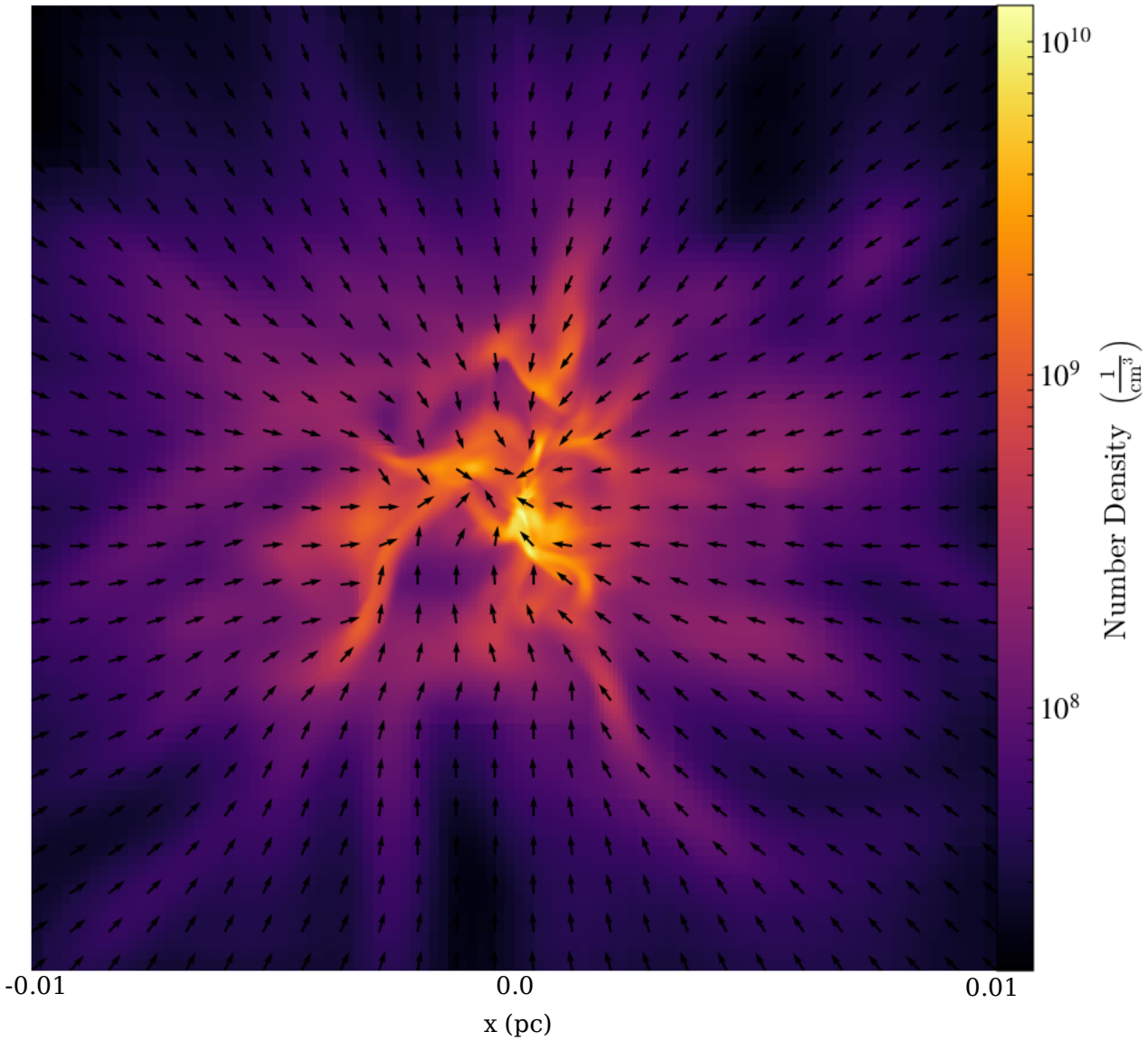

Figure 4.1: A cross section of the core through its central (x, y) plane at $t \approx t_{\text{ff}}$, showing the velocity vectors.

Chapter 5

Results

5.1 Measurements

The presence of the initial Gaussian density profile with the maximum at the center of the simulation box causes the collapse to focus onto this point, and also causes the collapse to adopt an approximately spherical symmetry. In what follows, we analyze only the central part of the core, where the density is nearly flat, and the inwards radial velocity increases linearly with the radius (e.g., Whitworth and Summers, 1985; Naranjo-Romero et al., 2015). Beyond this radius, the velocity begins to decrease again, as also observed in Keto and Caselli (2010) and Naranjo-Romero et al. (2015).

Note that in this section we will consider the infall speed of the non-turbulent run as the effective value of $v_{\rm g}$, the gravitational velocity, rather than the value given by eq. (3.1). This is because, in practice, a marginally unstable isothermal sphere collapses at a rate significantly lower than the free-fall rate, since the thermal pressure is never negligible (see Appendix C of Larson, 1969), and so the actual infall speed is lower than the free fall value. Thus, in what follows, we will refer to the infall speed of the non-turbulent run simply as the infall (or gravitational) speed denoted by $v_{\rm g,sim}$.

To separate the infall component from the turbulent components, we follow the procedure used by Vázquez-Semadeni et al. (1998), and convert the grid from Cartesian to spherical coordinates to separate the radial ($v_{\rm rad}$) and the tangential components (v_φ and v_θ), which we will assume represents only the turbulent velocity. Then, the tangential velocity satisfies eq. (3.2), and we assume that it represents the one-dimensional turbulent velocity dispersion; i.e., that

$$\sigma_{\rm 1D}^2 \equiv \langle v_{\rm tan}^2 \rangle. \tag{5.1}$$

We then average the density as well as the radial and tangential velocity components over

spherical shells of width equal to one cell, and compute these averages as a function of the radial distance from the center of the collapse.

Figure 5.1 shows the radial profile of the infall velocity at various times for the fiducial turbulent run (turb 08) and for the non-turbulent one. The inner region where the inwards velocity is approximately linear with radius (Whitworth and Summers, 1985) is clearly seen, and is seen to become smaller as time progresses. As shown by those authors, the density profile is nearly flat over this region, whose extent is approximately one Jeans length of the central density (Keto and Caselli, 2010). The infall speed is thus maximum at the edge of the central flat region. In what follows, we consider the infall speeds of the simulations at half the radius of this central, flat-density region. In the turbulent simulations, its extent is determined by angle-averaging the radial velocity at each radius. This procedure averages out the turbulent component, and thus only the infall component remains.

To avoid contamination from the boundary conditions, we only consider the radial dependence of the velocities within this region, which radius is resolved at all times by 12 or 24 cells during the contraction, as required by the refinement criterion in the low- and high-resolution simulations, respectively.

An important point to note from Fig. 5.1 is that the radial velocity profile of the turbulent run at each timestep is very similar to that of the nonturbulent run, implying that the collapse in the presence of turbulence occurs at the same rate as in the nonturbulent case. We discuss the implications of this result in Sec. 6.1.

Figure 5.2 shows the evolution of the ratio of the average of the radial velocity dispersion $\langle v^2_{\rm rad}(r_{1/2})\rangle^{1/2}$ at half the radius of the flat-density region in the turbulent runs to the infall speed v_g at the same position in the non-turbulent run. We observe that, at early times, the ratio is rather large, because the turbulent velocity dispersion is largest, while the infall speed is very small. On the other hand, at larger times, the ratio appears to saturate at a value $f \approx 1.062$.

Fig. 5.3 shows the evolution of the ratio $h^2_{\rm sim} = \langle v^2_{\rm tan}\rangle/\langle v^2_{\rm rad}\rangle$ of the square of the tangential velocity to the square of the radial velocity in the simulation, or, equivalently, the ratio of the 1D turbulent velocity dispersion to the total inwards kinetic energy, $\sigma^2_{\rm 1D}/\langle v^2_{\rm rad}\rangle$, both measured at half the radius of the flat-density region. It is seen that this ratio first decreases, and then apparently tends to approach stationarity at a value $h^2_{\rm sim} \approx 0.164$. This apparent stationarity is observed in proto-stellar analytical and numerical studies (Murray and Chang, 2015; Murray et al., 2017).

The evolution of this ratio can be understood considering that the tangential velocity dispersion contains only the turbulent contribution, while the radial velocity dispersion contains this contribution plus that from infall. At the initial condition (not shown in Fig. 5.3), the gravitational velocity is zero, so that $\langle v^2_{\rm rad}\rangle = \sigma^2_{\rm 1D}$, and thus $h^2_{\rm sim} = 1$. After that, the initial

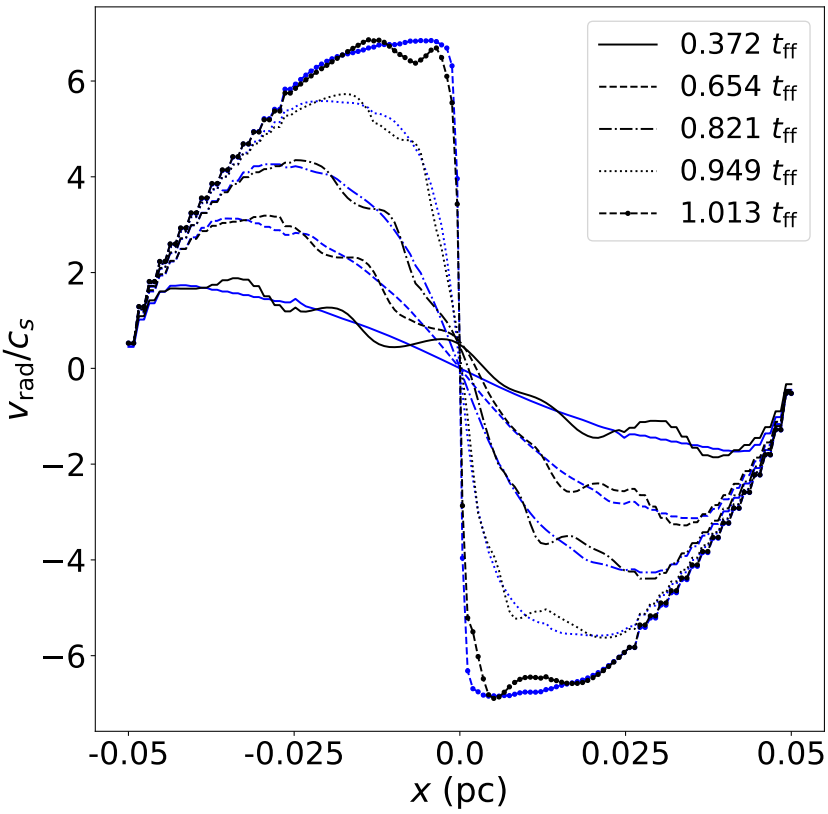

Figure 5.1: Radial velocity profiles of run turb 08 (black lines) and of the non-turbulent run (blue lines) at different times. Except for the random fluctuations in the turbulent case, the two simulations are seen to have the same mean radial velocity at all times.

decrease of this ratio indicates that the gravitational speed increases faster than the turbulent velocity dispersion.

On the other hand, the final, apparent nearly stationary value of the ratio $h^2_{\rm sim} \approx 0.164$ in Fig. 5.3 indicates that, at that level, the energy injection from the infall into the turbulence balances the turbulent dissipation, as considered in Sec. 3.3.

From these measurements, we can estimate g in two different ways. On one hand, from the second equality in eq. (3.6), we have

$$g_{\rm sim,1} = \sqrt{f^2_{\rm sim} h^2_{\rm sim}} \approx 1.062\,(0.164)^{1/2} \approx 0.43, \tag{5.2}$$

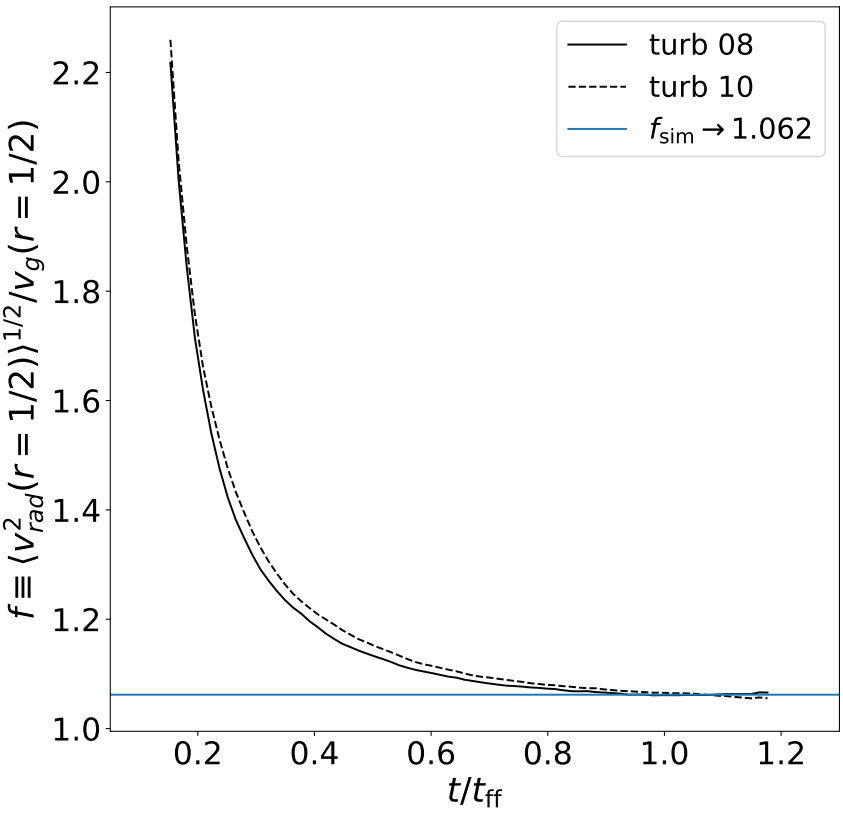

Figure 5.2: Evolution of the ratio of the radial velocity dispersion (i.e., the average of the squared radial component of the velocity) at half the radius of the flat-density region in the turbulent runs to the dispersion of the infall speed at the same radial position in the non-turbulent run.

on the other hand, we can also determine $g_{\rm sim}$ by dividing eq. (3.3) by $\langle v_{\rm rad}^2 \rangle$ to obtain

$$1 = h^2 + \frac{1}{f_{\rm sim}^2} = \frac{g^2+1}{f^2},$$

so that

$$g_{\rm sim,2} = \sqrt{f_{\rm sim}^2 - 1} \approx 0.36. \tag{5.3}$$

We see that the values of $g_{\rm sim}$ given by eqs. (5.2) and (5.3) are similar but not equal. This is probably an indication that our working hypotheses, for example, eqs. (3.2) and (3.3), apply only approximately. In this case, we can interpret the difference between the two estimates as giving the range of uncertainty of our measurements, and so we write

$$g_{\rm sim} = 0.395 \pm 0.035, \tag{5.4}$$

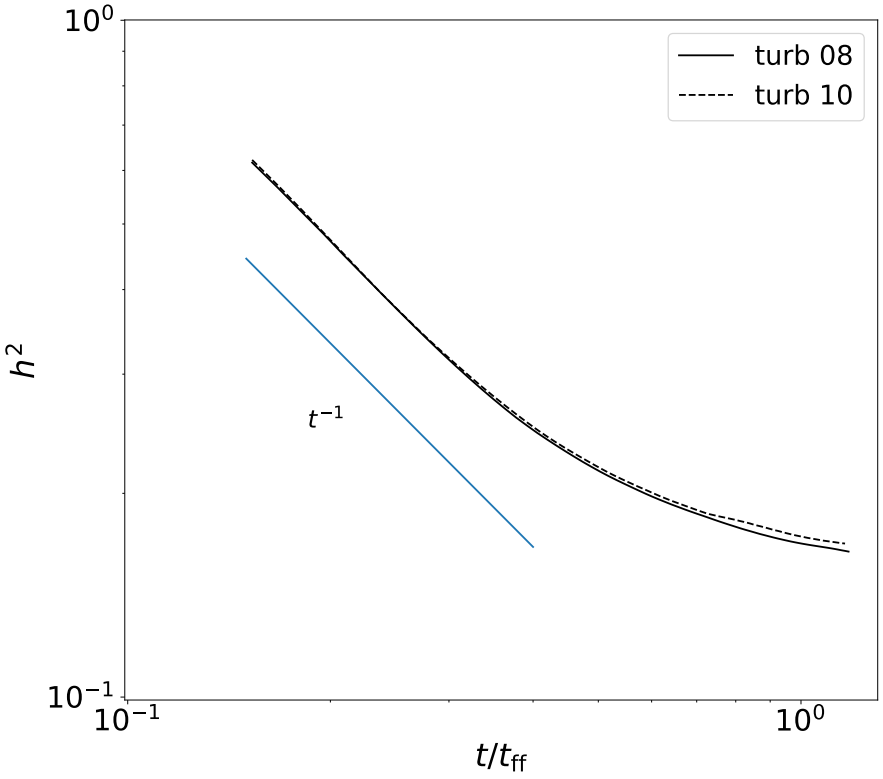

Figure 5.3: Evolution of the ratio of the 1D turbulent velocity dispersion squared to the angle-averaged radial velocity squared, both measured at half the radius where the maximum infall velocity occurs, for the two turbulent simulations. The ratio first decreases as a power law of time with slope ~ -1, and then it is seen to approach a stationary value $v_{\rm tan}^2/v_{\rm rad}^2 \approx 0.164$ by $t \approx t_{\rm ff}$ (as shown in Fig. 5.4).

It is noteworthy that this value is very similar to that expected in virial equilibrium (cf. eq. [3.11]), in spite of the fact that our core is collapsing essentially at the speed of the non-turbulent run. That is, there is no slowing down of the collapse by the turbulence generated, in spite of it being nearly at the virial value. We discuss the possible interpretation of this result in Sec. 6.1.

In addition, since the energy ratio attains a nearly stationary value, we can use eq. (3.17) to estimate $\mathcal{L}_{\rm d}/(\eta R) \approx 9.85$ for our system. According to Fig. 5.1, $\langle v_{\rm rad}\rangle/v_{\rm g} \approx 1$ by the end of the simulation, and so eq. (3.17) reduces to

$$\frac{\mathcal{L}_{\rm d}}{\eta R} \approx 4\pi\sqrt{3}\, g_{\rm sim} \approx 8.60 \pm 0.76. \tag{5.5}$$

We discuss the implications and possible interpretations of this result in Sec. 6.1.1.

5.1.1 Convergence study

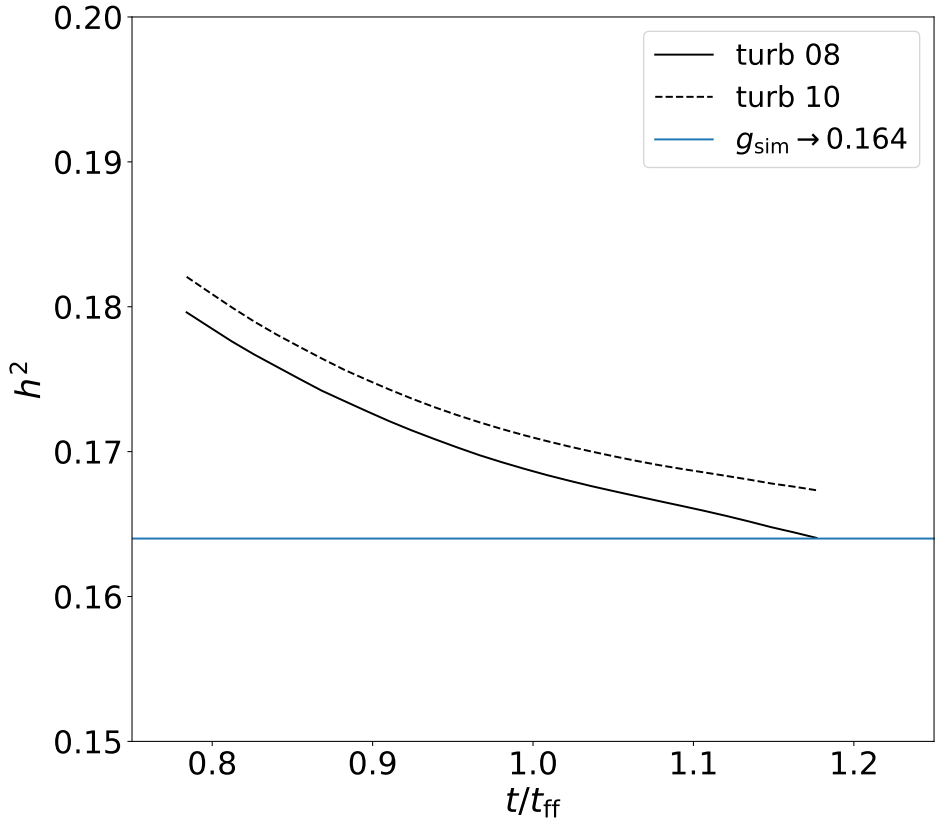

Figure 5.4: Zoom of the h^2 ratio for the final times. The solid line represents the run with a maximum refinement level of 8, the dashed line represent the run with a maximum refinement level of 10, and the blue line show the final value.

In order to test the reliability of our results upon changes in resolution, we performed an additional simulation "turb 10", in which we increased the maximum refinement level two levels above the fiducial run "turb 8" (cf. Table 4.1), and the number of cells per Jeans length in the refinement criterion is doubled to 24. The dashed line in Fig. 5.2 shows the evolution of the ratio of the root mean square radial velocity $\langle v_{\rm rad}^2 \rangle$ at the radius where the infall speed is maximum in the high-resolution turbulent run to the same quantity in the non-turbulent simulation. It is seen that this ratio remains within 1% of the value obtained for the low-resolution run (solid line), implying that our results are very well converged, and that the collapse time is real, rather than an artifact of numerical dissipation.

Chapter 6

Discussion

6.1 Implications

6.1.1 The injection scale and the dissipation efficiency

The analytical study of Sec. 3 provided us with a range of expected values for the velocity ratio g in the cases of energy equipartition (eq. [3.10]), virial balance (eq. [3.11]), and a self-consistent stationary state (eq. [3.17]). In particular, equating eq. (3.17) to the value obtained in our simulation, eq. (5.4), and recalling that $\langle v_{\rm rad}\rangle/v_{\rm g} \approx 1$ in our simulation, we find

$$\frac{\mathcal{L}_{\rm d}}{R} \approx 0.395 \times 4\sqrt{3}\pi\eta \approx 8.60\eta. \tag{6.1}$$

This equation can be interpreted in various ways. We can either assume that $\eta = \eta_{\rm ML}$ and determine the implied ratio of $\mathcal{L}_{\rm d}/R$, or else we can assume that $\mathcal{L}_{\rm d} = R$ and infer the corresponding value of η for our problem. A third option is to assume neither one of the previous possibilities, and take eq. (6.1) as the final result from our study. For the first two cases, we find:

Case I: $\eta = \eta_{\rm ML}$. In this case, we obtain

$$\mathcal{L}_{\rm d} \approx 0.57R, \tag{6.2}$$

implying that the driving scale is even smaller than the radius, contrary to the assumption made by Li (2018), that $\mathcal{L}_{\rm d} \sim 2R$.

Case II: $\mathcal{L}_{\rm d} = R$. In this case, we obtain

$$\eta_{\rm sim} \approx 0.12, \tag{6.3}$$

within a factor of 2 with respect to that reported by ML99, $\eta_{\rm ML} \approx 0.067$ (cf. Sec. 3.3).

It is not obvious which one of these two possible interpretations may be more realistic. On the one hand, it is reasonable to assume that the energy injection scale is of the order of the radius, but somewhat smaller, since all points in the core will traverse a distance equal to their respective radial positions by the end of the collapse, and these distances are equal or smaller than the radius of the entire core. On the other hand, it is also reasonable to assume that the dissipation efficiency will be of the order of that found by ML99, but not quite equal, since the nature of the driving mechanism, the geometry, and the numerical codes are different. All in all, probably the most appropriate conclusion is that the injection scale is of the order of the radius, and that the dissipation efficiency is of the same order as that reported by ML99.

6.1.2 The non-adiabatic nature of the turbulence driving by collapse

The generation of turbulence by gravitational collapse is often referred to as an "adiabatic heating" of the turbulence (e.g., Robertson and Goldreich, 2012; Murray and Chang, 2015; Li, 2018; Xu and Lazarian, 2020; Mandal et al., 2020). Although this terminology arises from the fact that, in the First Law of Thermodynamics ($dU = dQ - dW$), the $P\,dV$ work corresponds to an adiabatic heating process ($dQ = 0$, then $dU = -P\,dV$), it is important to keep in mind that turbulence is inherently a dissipative process, and so the net driving (or "heating") of the turbulence is far from being adiabatic, a term which, by definition, implies that no loss of heat or mass occurs during the process. Instead, in the case of turbulence, the dissipative loss of turbulent kinetic energy is unavoidable since, contrary to the case of microscopic molecular motions, in which particle collisions are ellastic, the "collision" of gas streams produce vortices and shocks where the kinetic energy is intrinsically converted to heat. This is in fact at the heart of the theory of Kolmogorov (1941), in which the slope of the turbulent energy spectrum is determined by the condition that the dissipation rate equals the injection rate and the energy transfer rate among scales.

The non-adiabatic nature of the turbulence generation by the collapse is manifested by the fact that the collapse does not appear to be significantly delayed by the turbulence, even though a nearly virial turbulent level is attained during the collapse. This can only be understood if the turbulent energy is dissipated as quickly as it is produced by the gravitational contraction, preventing it from delaying the collapse, contrary to the case of truly nearly adiabatic heating of a collapsing protostellar object when it becomes optically thick, trapping the heat, and producing a first hydrostatic core. Instead, our simulations suggest that no such halting, or even delaying, of the collapse is accomplished by the turbulence even when it appears virialized, fed by the collapse itself. This further implies that, in particular, when writing the virial theorem for a collapsing object including a nonthermal kinetic energy term (e.g., McKee and Zweibel,

1992; Ballesteros-Paredes et al., 1999; Ballesteros-Paredes, 2006; McKee and Ostriker, 2007), an additional term must be included to represent viscous dissipation of the turbulent energy. We plan to investigate this issue in the future.

The lossy character of the turbulent "heating" can also be seen in the effective polytropic exponent displayed by the turbulent and infall ram pressures, respectively defined as $P_{\rm t} \equiv \rho\sigma_{\rm 1D}^2$ and $P_{\rm r} \equiv \rho v_{\rm rad}^2$. The solid and dashed lines in Fig. 6.1 show these pressures, averaged over spherical shells, *versus* the corresponding average density in the shells. The blue line shows a slope of $\gamma_{\rm e} \sim 1.64$. This result is consistent with the study by Vázquez-Semadeni et al. (1998) who, using a spectral code to simulate a turbulent gravitational collapse, found values of the polytropic exponent $\gamma_{\rm e} \approx 3/2$ for nonmagnetic and rapidly collapsing magnetized cases, and $\gamma_{\rm e} \approx 2$ for slowly collapsing, strongly magnetized cases.

Also, it is noteworthy that this slope is very similar to the value of the polytropic exponent corresponding to an adiabatic process in a monoatomic gas, $\gamma = 5/3$, which in particular is larger than the well known critical value of 4/3 required for the internal thermal energy to be capable of halting gravitational collapse (e.g., Chandrasekhar, 1961; Vazquez-Semadeni et al., 1996). Nevertheless, **the turbulence turns out to be incapable of storing the energy of the collapse and thus delaying it to any significant extent**. The solution lies in the observation that the ram pressure is always larger than the turbulent one, showing that the turbulent energy, although continuously increasing, is always lagging behind the infall kinetic energy, a result which can only be attributed to the rapid dissipation and to the establishment of equality between the rates of collapse and of turbulent energy transfer. The fact that the result is preserved at higher resolution suggests that this is a real effect and not just an effect of excessive numerical dissipation.

6.1.3 Comparison with previous work

The problem of turbulence driving ("heating") by gravitational collapse has been addressed by a number of authors using both analytical and numerical approaches. Numerically, Vázquez-Semadeni et al. (1998) used a very similar approach to the one used here, except with a fixed-grid spectral code, to investigate the effective equation of state of the turbulence. In particular, Vázquez-Semadeni et al. (1998) were searching for a "logatropic" behavior (Lizano and Shu, 1989) of the turbulent pressure upon the compression produced by the collapse, but instead found a polytropic behavior with an effective exponent in the range 3/2–2 depending on the collapse regime. The exponent we find here (Fig. 6.1) is within the range determined by those authors.

More recently, other studies (Robertson and Goldreich, 2012; Mandal et al., 2020) have used numerical simulations of turbulent boxes using shrinking comoving coordinates, to investigate

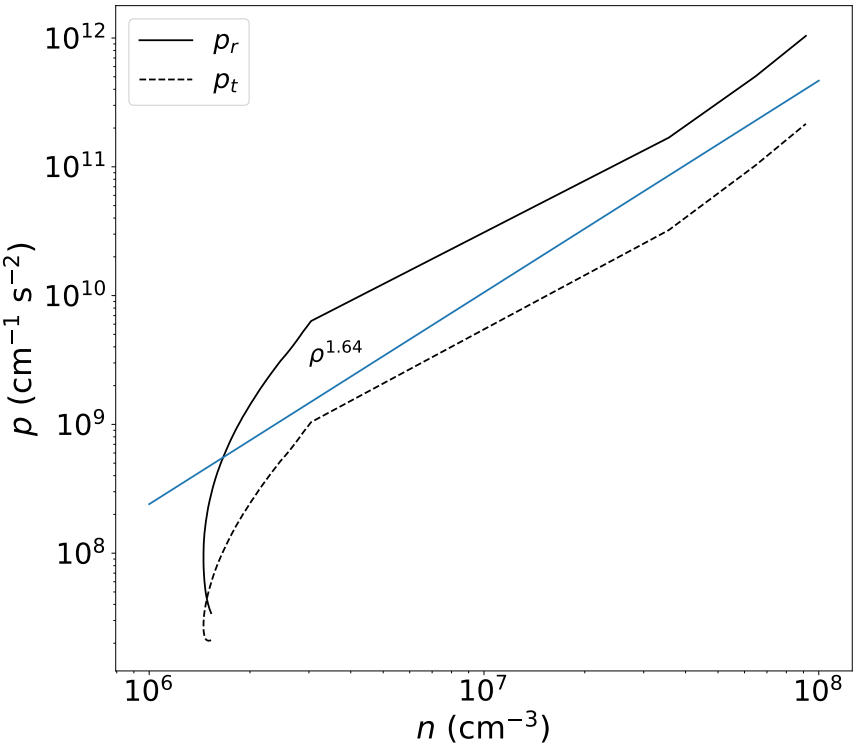

Figure 6.1: The solid line represents the ram pressure, the dashed line represents the turbulent pressure, and the blue line is a power law with a slope of 1.64.

the rate of turbulent generation during contraction. However, since in these simulations the contraction rate is a fixed parameter, they do not allow to self-consistently determine whether the collapse can be delayed or not by the turbulent pressure. Instead, assuming an isothermal gas, and considering also a model equation for the energy injection and dissipation balance, Robertson and Goldreich (2012) concluded that regardless of whether the turbulent transfer rate is initially larger or smaller than the contraction rate, the former approaches the latter. Our result that the turbulence approaches a "virial" value is in qualitative agreement with theirs. Similarly, using a thermally bistable gas, Mandal et al. (2020) found that the physical properties of the dense clouds in their simulations best matched those of real molecular clouds when the two rates are equal, again pointing towards a balance between the two rates in molecular clouds, in agreement with our results here.

From the analytical standpoint, various works have considered an energy balance equation for the energy injection from the contraction and the turbulent energy dissipation to compute the turbulent velocity dispersion, and from there compute a turbulent pressure which is added to the regular thermal pressure in the momentum equation for the infall speed (Robertson

and Goldreich, 2012; Murray and Chang, 2015; Li, 2018; Xu and Lazarian, 2020), with various results. As mentioned above, Robertson and Goldreich (2012) concluded that the turbulent transfer rate must approach the contraction rate. On the other hand, Murray and Chang (2015) consider a *protostellar* (or post-singularity) core, in which a central star or cluster has already formed, and define two distinct radial regions, separated by the radius that demarks the sphere of influence of the mass accreted onto the central object. They then conclude that "turbulent pressure" is important at all radii, and that the infall speed is smaller (resp. comparable) than the turbulent velocity outside (resp. inside) that radius. Since our simulations are restricted to the *prestellar* stage (i.e., pre-singularity), we cannot assess whether our simulations support their analytical result.

In addition, Xu and Lazarian (2020, hereafter XL20) have performed a similarity analysis of the "inside-out" collapse problem (Shu, 1977), in which they consider a fixed ratio C of the turbulent velocity (equivalent to our $v_{\rm tan}$ and $\sigma_{\rm 1D}$) to the total radial velocity (equivalent to our $v_{\rm rad}$), so their C is equivalent to our h. Under the assumption of a constant C, XL20 consider cases with different initial values of the ratio of the infall speed to the sound speed, and find that, when this ratio is initially large, significant (supersonic) turbulent energy is generated by the collapse, and that this turbulence has the effect of modifying the radial density and velocity profiles. The resulting infall velocity is uniform at large radii, it decreases inwards at intermediate radii, and then increases inwards at small radii. This infall velocity profile is actually somewhat similar to the classical prestellar profile, which has uniform velocity at large radii, and a linearly decreasing velocity at small radii (Whitworth and Summers, 1985, see also Fig. 5.1), with the difference that the velocity increases at small distance from the center. From these results, XL20 conclude that the turbulent pressure can slow down the collapse in the case of an initially large infall speed.

However, the general approach of considering the generation and dissipation of turbulence by the collapse and then feeding it back via a turbulent pressure term in the momentum equation has a number of important caveats, as we now discuss.

First, this approach implicitly assumes that the turbulent motions occur at such a small scale that they can be considered analogous to the thermal velocity dispersion of the gas molecules, neglecting the fact that the largest turbulent speeds occur at the largest scales within the system. Therefore, the effect of the turbulence is not to act as an isotropic pressure, but rather as a distorting agent for the density structures (Ballesteros-Paredes et al., 1999). As a consequence, rather than slowing down a monolithic collapse, large turbulent velocities (larger than the infall speed) are expected to cause fragmentation, shearing or compression of the collapsing core. XL20 explicitly state that, contrary to the case of turbulence driven by external compressions, for collapse-generated turbulence, the driving scale $\mathcal{L}_{\rm d}$ is small. However, our result that $\mathcal{L}_{\rm d} \lesssim R$

implies that it is still of the order of the radius of the collapsing core itself, so it is not small compared to the system size. On the other hand, it is not as large as the core's diameter, in contradiction to the *ad hoc* assumption of Li (2018), which was important for the conclusion by this author that the collapse can be retarded by the turbulence.

Within the framework of turbulent pressure support, both Murray and Chang (2015) and XL20 argue that its effect is to modify the velocity dispersion-size relation from the standard Larson (1981) form, $\sigma \propto R^{1/2}$, to scalings with significantly smaller exponents ~ 0.2 – 0.3. Both groups propose this as an explanation of the observation that dense massive cores often exhibit flatter scalings than Larson's (e.g., Caselli and Myers, 1995; Plume et al., 1997; Shirley et al., 2003; Gibson et al., 2009; Wu et al., 2010, as plotted by Ballesteros-Paredes et al. 2011). However, both Murray and Chang (2015) and XL20 have neglected the fact that those massive cores do follow the appropriate gravitational scaling once the additional dependence on the column density ($\sigma \propto \sqrt{\Sigma R}$; Keto and Myers, 1986; Heyer et al., 2009), is taken into account, as shown by Ballesteros-Paredes et al. (2011, see also Camacho et al. 2016; Ballesteros-Paredes et al. 2018). Those, the apparent deviations from Larson's linewidth-size relation can be fully accounted for by gravitational contraction when the column density dependence is included, with no need for turbulent support.

Second, in the similarity studies, the ratio of the contraction rate to the turbulent transfer rate is a parameter defined as an initial condition, because, by their very nature, similarity methods may not be consistent with the initial and boundary conditions of the problem (e.g., Shu, 1992, Ch. 17), and the solutions only apply once the initial transients have passed. However, it is precisely those initial transients that determine in a self-consistent manner the parameters of the similarity treatments. In this sense, our numerical simulations do evolve self-consistently from a much earlier stage than those considered by Shu (1977), Murray and Chang (2015) and XL20. In particular, it covers the period during which XL20's C parameter is not constant, and evolves toward its stationary value. Indeed, our turbulent simulations suggest a evolution towards a constant value of C (our h), $\sim \sqrt{0.164} \approx 0.405$ (cf. Sec. 5.1), in agreement with XL20's assumption for the late-time evolution. At those late stages of our *prestellar* collapse, the infall speed is large compared to the sound speed (cf. Fig. 5.1) and there has been significant turbulent generation (as indicated by its nearly virial value; cf. eq. [5.4] and the subsequent discussion), also in agreement with Case 2 of XL20. Nevertheless, we do not observe any significant retardation of the collapse at any time nor radius. We speculate this is because our simulation evolves towards equality of the injection and dissipation rates, in which case XL20 find that the infall is undisturbed.

6.2 Caveats

Our work is certainly limited by some caveats. First, we have chosen to use an adaptive-mesh scheme in order to self-consistently be able to follow the collapse, in particular whether it is delayed by the turbulence generated. This cannot be accomplished using a fixed-resolution box with shrinking coordinates, as done by Robertson and Goldreich (2012) and Mandal et al. (2020), since in that case, the contraction rate is imposed as an external parameter. However, our choice implies that, at late stages, our core is only moderately resolved, possibly generating excessive numerical dissipation. Our high-resolution simulation, with twice the resolution in the core, still collapses in essentially the same time, and converges to nearly the same values of the velocity ratios, suggesting our result is robust. Nevertheless, it would be desirable to perform a test at much higher resolution, which we will attempt in a future study.

Second, we have chosen to use a very low level of initial turbulence in order to avoid the destruction of the core by the initial turbulence and thus approximately maintain the global spherical symmetry. It could be argued that this is the reason the collapse is not delayed. However, the fact that by the end of the turbulent simulations the turbulence has reached a nearly virial value, suggests that at those late stages the turbulence should be able to slow down the collapse. The fact that is does not strongly indicates that it is dissipated as rapidly as it is generated, which is in fact what we observe: a tendency to approach a stationary balance between injection and dissipation.

Third, we are not taking into account the role of the magnetic field. The role of the magnetic field in the collapsing core problem is likely to be important in the efficiency of turbulence driving by the collapse, although it may not be the dominant component, since it is now established that most molecular clouds and their cores are magnetically supercritical (Crutcher, 2012). But even in this case, magnetic fields may have two opposite effects in the efficiency of turbulence generation. On the one hand, the magnetic field could propagate the fluctuations via Alfvén waves, aiding the transfer of turbulent kinetic energy throughout the core. On the other hand, if the magnetic field is strong enough, it may restrict the velocity field to be oriented preferentially along field lines, inhibiting transverse motions. Since the collapse causes an hourglass (nearly radial) morphology of the field lines, the tangential motions in our core might be inhibited, thus inhibiting the transfer of energy from the radial collapse direction to the random turbulence. We plan to investigate the competition between these effects in a forthcoming study.

Finally, our simulations have been limited to the prestellar (pre-singularity formation) stage of the collapse, and so they are not directly comparable to some of the studies presented by some other groups, which consider the protostellar stage, with a finite-mass central point object already present (e.g., Murray and Chang, 2015). However, since the prestellar stage sets the

initial conditions for the formation of a protostar, we consider that understanding this stage is of utmost importance. In any case, in a future study we will attempt to follow the entire evolution from the prestellar to the protostellar stage.

Chapter 7

Summary and Concusions

In the present thesis, we have performed some simple analytical calculations predicting the ratio g of the one-dimensional turbulent velocity dispersion $\sigma_{1\mathrm{D}}$ to the gravitational velocity v_{g} under the conditions of free-fall (or energy equipartition, $E_{\mathrm{turb}} = |E_{\mathrm{g}}|$), virial balance ($2E_{\mathrm{turb}} = |E_{\mathrm{g}}|$) and a stationary balance between energy injection by the collapse and energy dissipation by viscosity. We then performed a suite of three numerical simulations of spherical collapse, two in the presence of initial turbulence at different resolutions, and one with no initial turbulence. We decomposed the velocity in radial and tangential components, identifying the latter with the purely turbulent one dimensional velocity dispersion $\sigma_{1\mathrm{D}}$. We then measured the ratio f as well as the ratio h of $\sigma_{1\mathrm{D}}$ to the mean square radial velocity $\langle v_{\mathrm{rad}}^2 \rangle^{1/2}$, and from there, we inferred the ratio g in the turbulent simulations by two different means.

In spite of our turbulence having a very small initial amplitude, we found that, before one free-fall time, the ratio $g = \sigma_{1\mathrm{D}}/v_{\mathrm{g}}$ has reached a nearly virial value $g_{\mathrm{sim}} = 0.395 \pm 0.035$. Nevertheless, we also found that $\sigma_{1\mathrm{D}}$ approaches a fixed fraction of the mean squared radial velocity, indicating a stationary balance between injection and dissipation. From here, we inferred the value of the dissipation efficiency η or the ratio of the energy injection scale $\mathcal{L}_{\mathrm{d}}$ to the core's radius, finding that η is within 70% of the value reported by ML99, and that $\mathcal{L}_{\mathrm{d}} \lesssim R$. Finally, we measured the effective polytropic exponent of the turbulent "pressure", finding a value $\gamma_{\mathrm{e}} \approx 1.64$, which, at face value, would suggest a nearly adiabatic character of the turbulent pressure upon compression.

Most important, however, is the fact that we did not find any significant slowing down of the collapse in neither of the turbulent simulations, compared to that of the non-turbulent simulation, in spite of $\sigma_{1\mathrm{D}}$ having a nearly virial value, and γ_{e} being larger than the critical value of $4/3$, above which a polytropic gas is capable of halting the collapse. This led us to conclude that the turbulence generated by the collapse is dissipated so rapidly (independently of resolution) that it is unable to delay the collapse at any significant rate. This implies that

neither the critical value $\gamma_e = 4/3$ nor the presence of a nearly virial velocity dispersion can be taken as indicative of delay or halting of the collapse in the presence of strong dissipation, which is equivalent to a loss of heat in a thermodynamic system. Therefore, the "heating" of turbulence by gravitational collapse is lossy rather than adiabatic, and that the dissipation of turbulence occurs at the same rate as the injection, implying that it cannot be stored in the system to slow down the collapse.

Chapter 8

Future Work

8.1 Gravitational Collapse Including Sink Particles

Thinking of continuing with this project, this can be improved by adding sink particles in the simulations, this is because numerical simulations of gravitational collapse with Eulerian codes, have the issue that at some point there is a large amount of fluid within a few cells, and this situation leads to numerical errors and the simulation can stop shortly after reaching free fall time.

In this process, an amount of gas above a certain density can convert into a singular point with the mass of the gas converted and can accrete material of the surroundings.

Also, we can run a set of numerical simulations changing the initial rms turbulence to test if this setup with a different kinetic energy acts in a similar way of stabilization between the injection and dissipations rates of the turbulence and near-virialization behave between the turbulent kinetic and the gravitational energy.

8.2 Virial Theorem Including Dissipation

In the Sec. 2.2 we take the Virial Theroem and solve it for an specific case of hydrostatic equilibrium where the internal energy provides support against self-gravity and a case with a turbulent velocity field that acts providing additional support in a similar way. But, in this last case, the kinetic energy of the turbulence is not constant in time if we take into account that the turbulence dissipates in roughly a crossing time (see e.g. Mac Low, 1999; Avila-Reese and Vázquez-Semadeni, 2001), so we need to consider a dissipation term by adding the viscosity of the fluid.

8.3 Signature of Collapse in Synthetic Spectral Lines

We made an analysis of the numerical simulations using the radiative transfer code RADMC-3D (Dullemond et al., 2012) following similar conditions to those used by Loughnane et al. (2018).

In this analysis, we extracted spectral lines of optically thin (N_2H^+) and thick (HCO^+) molecules at the $J = 3 - 2$ transition assuming a constant abundance and taking the density and velocity profiles to find the assymetry of this molecular lines due to the gravitational collapse described and obtained in observations and numerical simulations (see e.g. Mardones et al., 1997; Smith et al., 2013; Loughnane et al., 2018).

We want to continue this analysis to compare our with the results of Loughnane et al. (2018) that used the simulations of Naranjo-Romero et al. (2015), with the main difference that their simulations do not have an initial turbulent field like our simulations, and to see the contribution of this ingredient.

Bibliography

Avila-Reese, V. and Vázquez-Semadeni, E. (2001). Turbulent Dissipation in the Interstellar Medium: The Coexistence of Forced and Decaying Regimes and Implications for Galaxy Formation and Evolution. *ApJ* , 553(2):645–660.

Balbus, S. A. and Hawley, J. F. (1991). A Powerful Local Shear Instability in Weakly Magnetized Disks. I. Linear Analysis. *ApJ* , 376:214.

Ballesteros-Paredes, J. (2006). Six myths on the virial theorem for interstellar clouds. *MNRAS* , 372(1):443–449.

Ballesteros-Paredes, J., Hartmann, L. W., Vázquez-Semadeni, E., Heitsch, F., and Zamora-Avilés, M. A. (2011). Gravity or turbulence? Velocity dispersion-size relation. *MNRAS* , 411:65–70.

Ballesteros-Paredes, J., Vázquez-Semadeni, E., Palau, A., and Klessen, R. S. (2018). Gravity or turbulence? - IV. Collapsing cores in out-of-virial disguise. *MNRAS* , 479(2):2112–2125.

Ballesteros-Paredes, J., Vázquez-Semadeni, E., and Scalo, J. (1999). Clouds as Turbulent Density Fluctuations: Implications for Pressure Confinement and Spectral Line Data Interpretation. *ApJ* , 515(1):286–303.

Bonazzola, S., Heyvaerts, J., Falgarone, E., Perault, M., and Puget, J. L. (1987). Jeans collapse in a turbulent medium. *A&A* , 172(1-2):293–298.

Bonnell, I. A., Bate, M. R., Clarke, C. J., and Pringle, J. E. (2001). Competitive accretion in embedded stellar clusters. *MNRAS* , 323(4):785–794.

Camacho, V., Vázquez-Semadeni, E., Ballesteros-Paredes, J., Gómez, G. C., Fall, S. M., and Mata-Chávez, M. D. (2016). Energy Budget of Forming Clumps in Numerical Simulations of Collapsing Clouds. *ApJ* , 833(1):113.

Caselli, P. and Myers, P. C. (1995). The Line Width–Size Relation in Massive Cloud Cores. *ApJ* , 446:665.

Chandrasekhar, S. (1961). *Hydrodynamic and hydromagnetic stability.*

Chomiuk, L. and Povich, M. S. (2011). Toward a Unification of Star Formation Rate Determinations in the Milky Way and Other Galaxies. *AJ* , 142(6):197.

Crutcher, R. M. (2012). Magnetic Fields in Molecular Clouds. *ARA&A* , 50:29–63.

Crutcher, R. M., Troland, T. H., Lazareff, B., Paubert, G., and Kazès, I. (1999). Detection of the CN Zeeman Effect in Molecular Clouds. *ApJL* , 514(2):L121–L124.

Dullemond, C. P., Juhasz, A., Pohl, A., Sereshti, F., Shetty, R., Peters, T., Commercon, B., and Flock, M. (2012). RADMC-3D: A multi-purpose radiative transfer tool.

Elmegreen, B. G., Elmegreen, D. M., Chand ar, R., Whitmore, B., and Regan, M. (2006). Hierarchical Star Formation in the Spiral Galaxy NGC 628. *ApJ* , 644(2):879–889.

Elmegreen, B. G. and Lada, C. J. (1977). Sequential formation of subgroups in OB associations. *ApJ* , 214:725–741.

Estalella, R. and Anglada, G. (1999). *Introducción a la Física del Medio Interestelar*. Edicions de la Universitat de Barcelona.

Ferrière, K. M. (2001). The interstellar environment of our galaxy. *Reviews of Modern Physics*, 73(4):1031–1066.

Field, G. B., Blackman, E. G., and Keto, E. R. (2008). A model of cloud fragmentation. *MNRAS* , 385(1):181–188.

Fryxell, B., Olson, K., Ricker, P., Timmes, F. X., Zingale, M., Lamb, D. Q., MacNeice, P., Rosner, R., Truran, J. W., and Tufo, H. (2000). FLASH: An Adaptive Mesh Hydrodynamics Code for Modeling Astrophysical Thermonuclear Flashes. *ApJS* , 131:273–334.

Gao, Y. and Solomon, P. M. (2004). The Star Formation Rate and Dense Molecular Gas in Galaxies. *ApJ* , 606(1):271–290.

Gibson, D., Plume, R., Bergin, E., Ragan, S., and Evans, N. (2009). Molecular Line Observations of Infrared Dark Clouds. II. Physical Conditions. *ApJ* , 705(1):123–134.

Goldreich, P. and Kwan, J. (1974). Molecular Clouds. *ApJ* , 189:441–454.

Heyer, M., Krawczyk, C., Duval, J., and Jackson, J. M. (2009). Re-Examining Larson's Scaling Relationships in Galactic Molecular Clouds. *ApJ* , 699:1092–1103.

Ho, Y.-C. and Cao, X.-R. (1991). *Perturbation analysis of discrete event dynamic systems.* Boston, MA etc.: Kluwer Academic Publishers.

Jeans, J. H. (1902). The Stability of a Spherical Nebula. *Philosophical Transactions of the Royal Society of London Series A*, 199:1–53.

Jijina, J., Myers, P. C., and Adams, F. C. (1999). Dense Cores Mapped in Ammonia: A Database. *ApJS* , 125(1):161–236.

Keto, E. and Caselli, P. (2010). Dynamics and depletion in thermally supercritical starless cores. *MNRAS* , 402(3):1625–1634.

Keto, E., Zhang, Q., and Kurtz, S. (2008). The Early Evolution of Massive Stars: Radio Recombination Line Spectra. *ApJ* , 672(1):423–432.

Keto, E. R. and Myers, P. C. (1986). CO Observations of Southern High-Latitude Clouds. *ApJ* , 304:466.

Klessen, R. S. (2011). Star Formation in Molecular Clouds. In Charbonnel, C. and Montmerle, T., editors, *EAS Publications Series*, volume 51 of *EAS Publications Series*, pages 133–167.

Klessen, R. S. and Glover, S. C. O. (2016). Physical Processes in the Interstellar Medium. *Saas-Fee Advanced Course*, 43:85.

Klessen, R. S. and Hennebelle, P. (2010). Accretion-driven turbulence as universal process: galaxies, molecular clouds, and protostellar disks. *A&A* , 520:A17.

Kolmogorov, A. (1941). The Local Structure of Turbulence in Incompressible Viscous Fluid for Very Large Reynolds' Numbers. *Akademiia Nauk SSSR Doklady*, 30:301–305.

Lada, C. J. (1985). Cold outflows, energetic winds, and enigmatic jets around young stellar objects. *ARA&A* , 23:267–317.

Lada, C. J., Gottlieb, C. A., Litvak, M. M., and Lilley, A. E. (1974). Molecular studies of two dark nebulae associated with Herbig-Haro objects. *ApJ* , 194:609–618.

Larson, R. B. (1969). Numerical calculations of the dynamics of collapsing proto-star. *MNRAS* , 145:271.

Larson, R. B. (1981). Turbulence and star formation in molecular clouds. *MNRAS* , 194:809–826.

Lemaster, M. N. and Stone, J. M. (2009). Dissipation and Heating in Supersonic Hydrodynamic and MHD Turbulence. *ApJ* , 691(2):1092–1108.

Lesieur, M. (2008). *Turbulence in Fluids*.

Li, G.-X. (2018). Scale-free gravitational collapse as the origin of ρ r^{-2} density profile - a possible role of turbulence in regulating gravitational collapse. *MNRAS* , 477:4951–4956.

Lizano, S. and Shu, F. H. (1989). Molecular Cloud Cores and Bimodal Star Formation. *ApJ* , 342:834.

Loughnane, R. M., Vázquez-Semadeni, E., and Naranjo-Romero, R. (2018). Synthetic Spectral Signatures from Isothermal Collapsing Gas and the Interpretation of Infall Profiles. *arXiv e-prints*, page arXiv:1808.04792.

Mac Low, M.-M. (1999). The Energy Dissipation Rate of Supersonic, Magnetohydrodynamic Turbulence in Molecular Clouds. *ApJ* , 524(1):169–178.

Mac Low, M.-M. and Klessen, R. S. (2004). Control of star formation by supersonic turbulence. *Reviews of Modern Physics*, 76:125–194.

Mandal, A., Federrath, C., and Körtgen, B. (2020). Molecular cloud formation by compression of magnetized turbulent gas subjected to radiative cooling. *MNRAS* , 493(3):3098–3113.

Mardones, D., Myers, P. C., Tafalla, M., Wilner, D. J., Bachiller, R., and Garay, G. (1997). A Search for Infall Motions toward Nearby Young Stellar Objects. *ApJ* , 489(2):719–733.

McKee, C. F. (1989). Photoionization-regulated Star Formation and the Structure of Molecular Clouds. *ApJ* , 345:782.

McKee, C. F. and Ostriker, E. C. (2007). Theory of Star Formation. *ARA&A* , 45:565–687.

McKee, C. F. and Ostriker, J. P. (1977). A theory of the interstellar medium: three components regulated by supernova explosions in an inhomogeneous substrate. *ApJ* , 218:148–169.

McKee, C. F. and Zweibel, E. G. (1992). On the Virial Theorem for Turbulent Molecular Clouds. *ApJ* , 399:551.

Mestel, L. and Spitzer, L., J. (1956). Star formation in magnetic dust clouds. *MNRAS* , 116:503.

Murray, D. W., Chang, P., Murray, N. W., and Pittman, J. (2017). Collapse in self-gravitating turbulent fluids. *MNRAS* , 465:1316–1335.

Murray, N. and Chang, P. (2015). Star Formation in Self-gravitating Turbulent Fluids. *ApJ* , 804:44.

Naranjo-Romero, R., Vázquez-Semadeni, E., and Loughnane, R. M. (2015). Hierarchical Gravitational Fragmentation. I. Collapsing Cores within Collapsing Clouds. *ApJ* , 814:48.

Norman, C. and Silk, J. (1980). Clumpy molecular clouds - A dynamic model self-consistently regulated by T Tauri star formation. *ApJ* , 238:158–174.

Plume, R., Jaffe, D. T., Evans, Neal J., I., Martín-Pintado, J., and Gómez-González, J. (1997). Dense Gas and Star Formation: Characteristics of Cloud Cores Associated with Water Masers. *ApJ* , 476(2):730–749.

Pokhrel, R., Myers, P. C., Dunham, M. M., Stephens, I. W., Sadavoy, S. I., Zhang, Q., Bourke, T. L., Tobin, J. J., Lee, K. I., Gutermuth, R. A., and Offner, S. S. R. (2018). Hierarchical Fragmentation in the Perseus Molecular Cloud: From the Cloud Scale to Protostellar Objects. *ApJ* , 853(1):5.

Price, D. J. and Federrath, C. (2010). A comparison between grid and particle methods on the statistics of driven, supersonic, isothermal turbulence. *MNRAS* , 406:1659–1674.

Robertson, B. and Goldreich, P. (2012). Adiabatic Heating of Contracting Turbulent Fluids. *ApJL* , 750:L31.

Shirley, Y. L., Evans, Neal J., I., Young, K. E., Knez, C., and Jaffe, D. T. (2003). A CS J=5–>4 Mapping Survey Toward High-Mass Star-forming Cores Associated with Water Masers. *ApJS* , 149(2):375–403.

Shu, F. H. (1977). Self-similar collapse of isothermal spheres and star formation. *ApJ* , 214:488–497.

Shu, F. H. (1992). *The physics of astrophysics. Volume II: Gas dynamics.*

Shu, F. H., Adams, F. C., and Lizano, S. (1987). Star formation in molecular clouds: observation and theory. *ARA&A* , 25:23–81.

Smith, R. J., Shetty, R., Beuther, H., Klessen, R. S., and Bonnell, I. A. (2013). Line Profiles of Cores within Clusters. II. Signatures of Dynamical Collapse during High-mass Star Formation. *ApJ* , 771(1):24.

Spitzer, L. (1978). *Physical processes in the interstellar medium.*

Stone, J. M., Ostriker, E. C., and Gammie, C. F. (1998). Dissipation in Compressible Magnetohydrodynamic Turbulence. *ApJL* , 508(1):L99–L102.

Tafalla, M., Myers, P. C., Caselli, P., and Walmsley, C. M. (2004). On the internal structure of starless cores. I. Physical conditions and the distribution of CO, CS, N_2H^+, and NH_3 in L1498 and L1517B. *A&A* , 416:191–212.

Truelove, J. K., Klein, R. I., McKee, C. F., Holliman, John H., I., Howell, L. H., and Greenough, J. A. (1997). The Jeans Condition: A New Constraint on Spatial Resolution in Simulations of Isothermal Self-gravitational Hydrodynamics. *ApJ* , 489(2):L179–L183.

Vázquez-Semadeni, E., Ballesteros-Paredes, J., and Klessen, R. S. (2003). A Holistic Scenario of Turbulent Molecular Cloud Evolution and Control of the Star Formation Efficiency: First Tests. *ApJL* , 585(2):L131–L134.

Vázquez-Semadeni, E., Cantó, J., and Lizano, S. (1998). Does Turbulent Pressure Behave as a Logatrope? *ApJ* , 492:596–602.

Vázquez-Semadeni, E., Gómez, G. C., Jappsen, A. K., Ballesteros-Paredes, J., and Klessen, R. S. (2009). High- and Low-Mass Star-Forming Regions from Hierarchical Gravitational Fragmentation. High Local Star Formation Rates with Low Global Efficiencies. *ApJ* , 707(2):1023–1033.

Vázquez-Semadeni, E., Palau, A., Ballesteros-Paredes, J., Gómez, G. C., and Zamora-Avilés, M. (2019). Global hierarchical collapse in molecular clouds. Towards a comprehensive scenario. *MNRAS* , 490(3):3061–3097.

Vazquez-Semadeni, E., Passot, T., and Pouquet, A. (1996). Influence of Cooling-induced Compressibility on the Structure of Turbulent Flows and Gravitational Collapse. *ApJ* , 473:881.

Whitworth, A. and Summers, D. (1985). Self-similar condensation of spherically symmetric self-gravitating isothermal gas clouds. *MNRAS* , 214:1–25.

Wilson, R. W., Jefferts, K. B., and Penzias, A. A. (1970). Carbon Monoxide in the Orion Nebula. *ApJL* , 161:L43.

Wright, N. J. (2015). The Kinematics of Star Formation: Theory and Observation in the Gaia Era. *arXiv e-prints*, page arXiv:1512.06854.

Wu, J., Evans, Neal J., I., Shirley, Y. L., and Knez, C. (2010). The Properties of Massive, Dense Clumps: Mapping Surveys of HCN and CS. *ApJS* , 188(2):313–357.

Xu, S. and Lazarian, A. (2020). Turbulence in a Self-gravitating Molecular Cloud Core. *ApJ* , 890(2):157.

Zuckerman, B. and Evans, N. J., I. (1974). Models of Massive Molecular Clouds. *ApJL* , 192:L149.